AGU PUBLICATIONS

JGR

Journal of Geophysical Research: Space Physics

RESEARCH ARTICLE
10.1002/2016JA023002

Key Points:
- Electric component dominant in driving radial diffusion
- Electric and magnetic components exhibit weak dependence on energy
- Uncertainty quantification for the total radiation diffusion coefficient

Correspondence to:
A. F. Ali,
ashar.ali@colorado.edu

Citation:
Ali, A. F., D. M. Malaspina, S. R. Elkington, A. N. Jaynes, A. A. Chan, J. Wygant, and C. A. Kletzing (2016), Electric and magnetic radial diffusion coefficients using the Van Allen probes data, *J. Geophys. Res. Space Physics*, *121*, 9586–9607, doi:10.1002/2016JA023002.

Received 26 MAY 2016
Accepted 3 AUG 2016
Accepted article online 6 AUG 2016
Published online 12 OCT 2016

Electric and magnetic radial diffusion coefficients using the Van Allen probes data

Ashar F. Ali[1], David M. Malaspina[1], Scot R. Elkington[1], Allison N. Jaynes[1], Anthony A. Chan[2], John Wygant[3], and Craig A. Kletzing[4]

[1]Laboratory for Atmospheric and Space Physics, University of Colorado Boulder, Boulder, Colorado, USA, [2]Department of Physics and Astronomy, Rice University, Houston, Texas, USA, [3]School of Physics and Astronomy, University of Minnesota, Minneapolis, Minnesota, USA, [4]Department of Physics and Astronomy, University of Iowa, Iowa City, Iowa, USA

Abstract ULF waves are a common occurrence in the inner magnetosphere and they contribute to particle motion, significantly, at times. We used the magnetic and the electric field data from the Electric and Magnetic Field Instrument Suite and Integrated Sciences (EMFISIS) and the Electric Field and Waves instruments (EFW) on board the Van Allen Probes to estimate the ULF wave power in the compressional component of the magnetic field and the azimuthal component of the electric field, respectively. Using L^*, *Kp*, and magnetic local time (MLT) as parameters, we conclude that the noon sector contains higher ULF Pc-5 wave power compared with the other MLT sectors. The dawn, dusk, and midnight sectors have no statistically significant difference between them. The drift-averaged power spectral densities are used to derive the magnetic and the electric component of the radial diffusion coefficient. Both components exhibit little to no energy dependence, resulting in simple analytic models for both components. More importantly, the electric component is larger than the magnetic component by one to two orders of magnitude for almost all L^* and *Kp*; thus, the electric field perturbations are more effective in driving radial diffusion of charged particles in the inner magnetosphere. We also present a comparison of the Van Allen Probes radial diffusion coefficients, including the error estimates, with some of the previous published results. This allows us to gauge the large amount of uncertainty present in such estimates.

1. Introduction

It is well known that the Van Allen radiation belts contain highly energetic particles including electrons with energies ranging from 100 keV to several MeV [*Tascione*, 1988; *Kivelson and Russell*, 1995; *Baumjohann and Treumann*, 1997; *Treumann and Baumjohann*, 1997; *Cravens*, 2004]. These energetic particles can be dangerous for human endeavors in space, causing damage to biological systems and sensitive spacecraft components [*Baker*, 2001]. Therefore, it is essential to understand how particles can be energized, transported, and lost in the Earth's magnetosphere. Particle interactions with magnetohydrodynamic (MHD) waves in the inner magnetosphere have received considerable attention, and *Friedel et al.* [2002], *Elkington* [2006], and *Shprits et al.* [2008a, 2008b] describe a number of mechanisms that have been proposed to explain the observed enhancement, energization, and loss of particle population in the outer radiation belt. One such mechanism is radial diffusion [*Fälthammar*, 1965, 1966a, 1966b, 1968].

Charged particles trapped in the inner magnetosphere undergo three distinct types of periodic motions due to the geometry of the geomagnetic field, each with a characteristic timescale well separated from the others. The first type of periodic motion is called the gyro motion with its timescale being on the order of a few milliseconds. The second type of periodic motion is the bounce motion of a charged particle as it bounces between two mirror points moving latitudinally along a magnetic field line, with the characteristic timescale being between a tenth of a second and a few seconds. The third type of periodic motion is the longitudinal drift of a charged particle around the Earth, with the characteristic timescale typically being a few minutes. With each type of periodic motion, there is also an associated constant of motion which is adiabatically conserved if the background fields are perturbed on timescales larger than the associated timescale. The first adiabatic invariant $M = p_\perp^2/2m_0B$ is associated with gyro motion, and it is conserved if the perturbations in the background fields are on timescales much longer than the gyro period of the particle. Here $p_\perp$, m_0, and B are the perpendicular component of the particle's momentum, the rest mass of the particle, and the strength

of the magnetic field, respectively. The second adiabatic invariant, $J = \int_{m_1}^{m_2} p_{\|} \mathrm{d}s$, is associated with the bounce motion of the particle where m_1 and m_2 are the two mirror points, $p_{\|}$ is the parallel component of the particle's momentum, and ds is the element of length along a magnetic field line. The third adiabatic invariant, $\Phi = \oint \mathbf{B} \cdot \mathrm{d}s$, represents the magnetic flux enclosed by the drift path of the particle. *Roederer and Zhang* [2014] define the quantity $L^* = -2\pi k_0/\Phi R_E$, where k_0 and R_E are the Earth's magnetic dipole and radius, respectively. This quantity is often much easier to work with because of the asymmetry of the geomagnetic field.

The ultralow-frequency (ULF) range is defined as 1.67 mHz–5 Hz where the subset 1.67 mHz–6.67 mHz is denoted Pc-5 [*Jacobs et al.*, 1964]. ULF waves can be generated by several mechanisms in the inner magnetosphere. There are internal processes such as mirror [*Hasegawa*, 1969] and drift [*Southwood et al.*, 1969; *Chen and Hasegawa*, 1991] instabilities in the plasma drifting into the inner magnetosphere. External processes generating power at ULF frequencies include shear flow instabilities along the magnetopause [*Cahill and Winckler*, 1992; *Mann et al.*, 1999; *Claudepierre et al.*, 2008], solar wind pressure variations [*Kivelson and Southwood*, 1988; *Claudepierre et al.*, 2009], and transient ion foreshocks [*Hartinger et al.*, 2013]. Pc-5 wave timescales result in the conservation of the first two adiabatic invariants while violating the third adiabatic invariant for a typical relativistic electron in the outer zone. This causes a net change in the particle's radial position and results in a net gain or loss of energy for the particle depending upon the direction of radial displacement. This mechanism is effective through a wave-particle interaction when ULF Pc-5 wave frequency is a multiple of the drift frequency of the particle. The resonance condition for this interaction is given by $\omega = m\omega_d$ with m being the azimuthal wave mode number and ω and ω_d being the wave frequency and the drift frequency of the particle, respectively [*Fälthammar*, 1965; *Schulz and Lanzerotti*, 1974]. If the interaction occurs with waves over a range of frequencies, then the radial displacement of the particle may become stochastic and can be described using diffusion theory. The theoretical framework for radial diffusion has been extended by including drift resonance interactions between electrons and both ULF toroidal and poloidal wave modes in an asymmetric geomagnetic field by *Elkington et al.* [1999, 2003].

The radial diffusion coefficient quantifies the mean square displacement of a collection of particles in the radial direction,

$$D_{LL} = \frac{\langle (\Delta L)^2 \rangle}{2\tau}, \tag{1}$$

with τ being a time period much longer than the drift period. The radial diffusion coefficient, being a measure of the radial diffusion rate, has been given much analytical treatment [*Fälthammar*, 1965, 1966a, 1966b, 1968]. It has been shown that perturbations in both the induced electric field (8/15 of the total magnetic flux variations) and the magnetic field (7/15 of the total magnetic flux variations) are important for radial diffusion of charged particles. The total radial diffusion coefficient is often estimated as the sum of the electromagnetic component (D_{LL}^M), which includes contributions from oscillations in both the magnetic and the induced electric field, and the electrostatic component ($D_{LL}^{E_{\mathrm{static}}}$), which includes contribution only from the convective electric field

$$D_{LL} = D_{LL}^M + D_{LL}^{E_{\mathrm{static}}}. \tag{2}$$

The *Fälthammar* [1965] formulation presents the radial diffusion coefficients as a function of the power spectral densities (PSDs) of the compressional component of the magnetic field and the azimuthal component of the electric field. Therefore, many studies have been conducted to estimate the PSDs and then to estimate the diffusion coefficients. PSD methods have included particle observations of a long time interval [*Frank*, 1965; *Newkirk and Walt*, 1968; *Lanzerotti et al.*, 1970; *Lyons and Williams*, 1975; *West et al.*, 1981; *Selesnick et al.*, 1997] and balloon campaigns for the electric field measurements [*Mozer*, 1971; *Holzworth and Mozer*, 1979]. Magnetic field power spectra have been estimated as a function of L [*Lanzerotti and Robbins*, 1973; *Lanzerotti and Morgan*, 1973; *Lanzerotti et al.*, 1978; *Arthur et al.*, 1978; *Huang et al.*, 2010b; *Tu et al.*, 2012] with a well-known study conducted by *Brautigam and Albert* [2000]. *Brautigam and Albert* [2000] presented analytic expressions for both the electromagnetic and the electrostatic components of the diffusion coefficients. Their study concluded that the electromagnetic component is dominant over the electrostatic component for high-energy particles in the outer radiation belt. *Brautigam et al.* [2005] used the electric field measurements from Combined Release and Radiation Effect Satellite (CRRES) to compute D_{LL}^E using L and Kp as parameters. We note here that even though *Brautigam et al.* [2005] used the *Fälthammar* [1965] diffusion coefficient formulation, they made no attempt to separate the inductive and the convective electric fields. They used

the total measured electric field to estimate D_{LL}^{E}[CRRES]. This is due to the fact that from single point measurements, it is not possible to separate the fields [*Brautigam et al.*, 2005, paragraph 13].

A more recent radial diffusion formulation is that by *Fei et al.* [2006]. Since they do not assume any relationship between the phases of the oscillations in the electric and the magnetic fields, they presented the expressions for the magnetic diffusion coefficient (D_{LL}^{B}), which includes only the contributions from magnetic field oscillations and the total electric diffusion coefficient ($D_{LL}^{E_{\text{total}}}$), which includes the contributions from the total electric field. The two components can then be summed to obtain the total diffusion coefficient

$$D_{LL} = D_{LL}^{B} + D_{LL}^{E_{\text{total}}}. \tag{3}$$

This formulation has been used in recent studies [*Huang et al.*, 2010b; *Ozeke et al.*, 2012; *Tu et al.*, 2012; *Ozeke et al.*, 2014; *Ali et al.*, 2015; *Liu et al.*, 2016] to estimate the radial diffusion coefficients. *Tu et al.* [2012] used global MHD simulations modeling the 8 March 2008 storm along with data from Time History of Events and Macroscale Interactions during Substorms (THEMIS) and GOES to validate the results and concluded that the electric diffusion coefficients were dominant in driving radial diffusion, contrary to the *Brautigam and Albert* [2000] results. *Ozeke et al.* [2012, 2014] used magnetic field measurements from Active Magnetospheric Particle Tracer Explorers (AMPTE) and GOES to estimate D_{LL}^{B}[Ozeke] and then mapped the ground-based magnetic PSDs to estimate D_{LL}^{E}[Ozeke]. Their conclusions were in agreement with *Tu et al.* [2012] that the magnetic field perturbations are not as important in driving radial diffusion as previously thought. *Ali et al.* [2015] used the CRRES magnetometer data along with the *Fei et al.* [2006] formulation to estimate D_{LL}^{B}[CRRES] and presented a comparison with some of the previous studies summarized as

$$D_{LL}^{B}[\text{CRRES}] \ll D_{LL}^{E}[\text{CRRES}] \leq D_{LL}^{E}[\text{BA}] \ll D_{LL}^{M}[\text{BA}]$$

where D_{LL}^{E}[BA] and D_{LL}^{M}[BA], respectively, denote the electrostatic and the electromagnetic components of the radial diffusion coefficients presented by *Brautigam and Albert* [2000]. *Liu et al.* [2016] used the electric field measurements from THEMIS-D to calculate the electric component of the radial diffusion coefficient which vary significantly from the *Brautigam and Albert* [2000], *Brautigam et al.* [2005], *Ozeke et al.* [2012], and *Ozeke et al.* [2014] estimates.

In this paper, we use the electric and the magnetic field data from Electric Field and Waves (EFW) and Electric and Magnetic Field Instrument Suite and Integrated Sciences (EMFISIS), respectively, on board the Van Allen Probes to first estimate the power spectral density in the compressional component of the magnetic field and the azimuthal component of the electric field. We then look at the ULF wave power distribution in both components in azimuth. We use the drift-averaged PSDs along with the *Fei et al.* [2006] formulation to estimate both the D_{LL}^{E} and D_{LL}^{B}. We use L^* [*Roederer and Zhang*, 2014] along with *Kp* as the activity-dependent parameter to parameterize both of the radial diffusion coefficients. This allows us to compare the relative contribution of both the electric and the magnetic component in driving radial diffusion. We also explore the L^* dependence of the radial diffusion coefficients and then present some analytical expressions for the diffusion coefficients. Finally, we compare our results using in situ measurements from the Van Allen Probes with previous diffusion coefficients estimates.

2. Radial Diffusion Formalism

Small random changes in the electric and magnetic field lead to a slow and gradual net change in a charged particle's position. This naturally suggests a diffusion framework. Diffusive transport of relativistic electrons can be modeled as the evolution of the phase space density in the coordinate space of the three adiabatic invariants with a Fokker-Planck equation [*Schulz and Lanzerotti*, 1974]. If the first and second adiabatic invariants are conserved while the third adiabatic invariant is violated, then the Fokker-Planck equation reduces to a one-dimensional diffusion equation

$$\frac{\partial f}{\partial t} = L^2 \frac{\partial}{\partial L}\left(\frac{D_{LL}}{L^2} \cdot \frac{\partial f}{\partial L}\right) \tag{4}$$

with f being the phase space density of electrons averaged over all drift phase angles and L denoting the L^* parameter [*Roederer and Zhang*, 2014].

Fälthammar [1965] used a diffusion formalism to derive the diffusion coefficients using only single-mode fluctuations which were valid only for nonrelativistic particles. *Fei et al.* [2006] later included the contributions from all azimuthal wave modes, made the additional assumption that the magnetic field perturbations and the inductive electric field perturbations have completely independent phases, and presented relativistically correct expressions for the magnetic and the electric diffusion coefficients as

$$D_{LL}^{B} = \frac{M^2 L^4}{8q^2 R_E^4 B_0^2 \gamma^2} \sum_{m=1}^{\infty} m^2 P_m^B(m\omega_d), \tag{5}$$

$$D_{LL}^{E} = \frac{L^6}{8B_0^2 R_E^2} \sum_{m=1}^{\infty} P_m^E(m\omega_d), \tag{6}$$

where R_E is Earth's radius, B_0 is the strength of the equatorial geomagnetic field at the Earth's surface, M is the relativistically correct first adiabatic invariant, L is the Roederer L^*, γ is the relativistic correction factor, q is the charge of the particle, ω_d is the drift frequency of the particle, and m is the azimuthal wave mode number. P_m^B and P_m^E are the power spectral densities of the compressional component of the magnetic field and the azimuthal component of the total electric field. With single-point in situ measurements in space and in time, it is very difficult to separate the total electric field into its inductive and convective components. Therefore, no such attempt has been made for this study. D_{LL}^{B}[RBSP] contains contributions only from the magnetic field oscillations while D_{LL}^{E}[RBSP] contains contributions from the total electric field. We assume here that all of the wave power is contained entirely in the first $m = 1$ mode. Equations (5) and (6) require summation of power over all wave mode numbers, but using single point measurements, we cannot ascertain the power distribution across different modes. In order to compute the power in mode m we would need at least $2m$ observations simultaneous in time such as those possible with a constellation of satellites. Therefore, for this study, we assume that the first ($m = 1$) mode contains all of the power and the power in all other modes is zero. *Brautigam et al.* [2005] and *Ali et al.* [2015] both made this assumption when working with the CRRES electric and magnetic field data, respectively. Furthermore, the *Fei et al.* [2006] formulation assumes that the ULF wave PSD is drift averaged. However, this may not be true in general as the distribution of ULF wave power in azimuth depends on the physical origin of ULF waves. For example, ULF waves originating due to Kelvin-Helmholtz instability tend to have higher wave power in dawn and dusk regions [*Claudepierre et al.*, 2008], while ULF wave activity due to solar wind pressure variations will have higher wave power on the dayside compared to the nightside [*Ukhorskiy et al.*, 2006; *Claudepierre et al.*, 2009; *Huang et al.*, 2010a].

3. Van Allen Probes Instruments

The Van Allen Probes, formerly known as Radiation Belt Storm Probes (RBSP), is a NASA mission dedicated to the study of Van Allen radiation belts. The mission consists of two identical spacecraft, launched on 30 August 2012. The initial mission duration was 2 years, plus an extended mission. The probes have nearly identical orbits, with perigee at approximately 500 km and apogee at approximately 30,000 km (5.7 R_E), an inclination of almost 10°, and an orbital period of about 9 h. Both probes are spin stabilized with the spin rate being about 5 rpm. The Electric and Magnetic Field Instrument Suite and Integrated Sciences (EMFISIS) on board each of the Van Allen Probes includes a triaxial fluxgate magnetometer with a dynamic range of 0.008 nT to 65,536 nT, providing the full magnetic field vector with a cadence of 64 measurements per second [*Kletzing et al.*, 2013]. The Electric Field and Waves (EFW) instruments on board each of the Van Allen Probes consists of four spin plane booms and two spin axis booms with probes at the boom tips to measure the ambient electric field. The spin plane component of the electric field is provided with the dynamic range being 0.05 mV/M to 1 V/m with a cadence of 32 measurements per second [*Wygant et al.*, 2013]. The spin fit level 2 electric field data contain only the E_y and E_z components in modified GSE (mGSE) coordinates. The mGSE coordinate system is defined with the x axis being the Van Allen Probes spin axis, which is always within 37° of the Sun-Earth line, the y axis intersecting the ecliptic and the spin plane and pointing toward dusk, and the z axis completing the coordinate system.

4. Data Preparation and Processing

The data used in this statistical study span 3 years, from September 2012 to August 2015. MLT refers to the magnetic local time of the spacecraft in eccentric dipole coordinates given in units of hours. L^* is the

Roederer L shell parameter [*Roederer and Zhang*, 2014] corresponding to a 90° pitch angle computed using the Tsyganenko storm time magnetic field model (TS04D) [*Tsyganenko and Sitnov*, 2005]. The activity-dependent parameter used for this study is the 3 h averaged *Kp* obtained from NASA's OMNI database. The index *Kp* was chosen over other activity indices, because it is a widely used planetary index indicative of magnetic activity on a global scale. Furthermore, the use of *Kp* facilitates comparison with other previous studies.

For the magnetic field data, we started with the level 3 (L3) EMFISIS fluxgate magnetometer data provided at 4 s resolution in solar magnetic (SM) coordinates for both RBSP-A and RBSP-B. After deleting orbits which were incomplete (i.e., the provided magnetometer data spanned an interval much smaller than 9 h), each magnetic field measurement was assigned the corresponding MLT, L^*, and *Kp* value using interpolation. At this point, all of the remaining orbits were inspected for spikes or invalid magnetic field measurements. Orbits with too many corrupted data points were removed while those with only a few corrupted points were fixed using interpolation. This was necessary because the subsequent Fourier analysis requires continuous data segments as well as to retain as much of the data as possible for a detailed statistical study. Since thruster firing events affect the fluxgate magnetometer readings, magnetic field measurements taken during spacecraft maneuvers were discarded. During the course of our study it was noted that after a thruster firing event, all three components of the magnetic field recorded a "ringing" which introduced spurious broadband wave power between 1 mHz and 4 mHz and sometimes persisted for several days. This ringing was not present in the compressional component of the magnetic field. Therefore, we delete only the orbits in which maneuvering occurred without deleting any additional orbits. This resulted in about a 4% data loss for each spacecraft.

The electric field data used for this study had 12 s resolution. Therefore, in order to make the comparison between the magnetic and the electric component of the diffusion coefficients easier, we decimated the magnetic field vector by a factor of 3, in order to degrade the time resolution from 4 s to 12 s. For this purpose, we digitally filtered all three components of the magnetic field using a low-pass infinite impulse response (IIR) filter so that there would not be any aliasing effects when we retain only every third data point [*Press et al.*, 2007]. Since we are only concerned with ULF wave power in the Pc-5 range (1.67 mHz–6.67 mHz), the decrease in Nyquist frequency from ~120 mHz to ~40 mHz was inconsequential. In order to estimate D_{LL}^{B}, we need to estimate the power spectral density of the compressional component of the magnetic field vector **B**, which in turn requires the variations in **B** in the direction of **B**, i.e.,

$$B_{\parallel} = \Delta\mathbf{B} \cdot \frac{\mathbf{B}}{\|\mathbf{B}\|} = (\mathbf{B} - \langle\mathbf{B}\rangle) \cdot \frac{\mathbf{B}}{\|\mathbf{B}\|} \tag{7}$$

where $\Delta\mathbf{B}$ are the variations we are interested in and can be subtracted from **B** to obtain the average ambient magnetic field $\langle\mathbf{B}\rangle$. In order to obtain $\Delta\mathbf{B}$, we employed a digital high-pass IIR filter after which we obtain $\langle\mathbf{B}\rangle$ and consequently the compressional component $B_{\parallel}$. Because of our focus on the ultralow-frequency range and the large ambient magnetic field combined with a large gradient of the magnetic field as the spacecraft moved inbound and outbound with high velocities at low L^*, it proved daunting to remove the static ambient field and to isolate the relatively small amplitude variations we were interested in. We therefore did not use any data with $L^* < 2.5$.

Consider a time series $x(t)$ for which we need to estimate the signal's power spectral density. If the time series is of finite length N with the sampling period Δt in seconds, then using the discrete Fourier transform, usually performed using the Fast Fourier Transform (FFT) algorithm to speed up the computations, results in a biased estimate of the periodogram because of the sharp truncation of the signal. If, however, the signal is first tapered (multiplied by a windowing function) which gradually goes to zero at the end points, then the periodogram bias can be reduced. Furthermore, in order to reduce the spectral variance, we can obtain several statistically independent periodograms of the signal $x(t)$ and then average them [*Press et al.*, 2007].

We employed the multitaper method to estimate the power spectral density which eliminates the need to use subsequences of $x(t)$ (usually overlapping) to reduce the spectral bias [*Thomson*, 1982]. The tapers (window functions) were mutually orthogonal vectors which provide statistically independent periodograms. These periodograms can then be averaged to obtain the final estimate. This method has the advantage of reducing both spectral bias and variance without sacrificing frequency resolution. The tapers used for this study were the Discrete Prolate Spheroidal Sequences (DPSS) also known as the Slepian sequences [*Slepian*, 1978] which can be calculated as the eigenvectors of a positive self-adjoint semidefinite symmetric tridiagonal matrix and may even take on negative values [*Press et al.*, 2007]. Since computing these eigenvectors can be

computationally expensive, the number of statistically independent tapers must be balanced between maximizing bias and variance reduction and computation time. In addition, higher-order DPSS are not zero at the endpoints so power leakage can be significant. For these reasons, we used the first seven tapers from DPSS in our spectral estimation. Using additional tapers showed no significant change in the power spectral density estimates.

We took data segments of length 20 min of the compressional component of the magnetic field and estimated the power spectral density using the multitaper method as described above. We chose the interval length of 20 min because that is how long the spacecraft typically take to cross an L^* bin of width 0.5 R_E. Since the resolution of data segments is 12 s, the resolved frequencies lie between ~0.825 mHz and ~40 mHz with the frequency step size being ~0.825 mHz. Since we only wish to consider the ULF Pc-5 range (1.67 mHz–6.67 mHz), we truncate the power spectral density estimates at ~8.25 mHz and ignore wave power at higher frequencies for the rest of this paper. After estimating the power spectral density of each data segment, we assigned the MLT, L^*, and *Kp* value corresponding to the central data point of each data segment and save them to be binned later.

For the electric field data, we started with the level 2 (L2) EFW data provided at 12 s resolution in the mGSE coordinate system for both RBSP-A and RBSP-B. Note here that only the E_y and E_z components of the electric field were available. After deleting orbits that were corrupted or incomplete, each electric field measurement was assigned the corresponding MLT, L^*, and *Kp* values using interpolation, and the two components were inspected for invalid values or unphysical spikes. Orbits with too much corrupted data were eliminated and the rest were fixed using interpolation so that we could have as much data as possible for our study. The electric field data are affected by spacecraft charging events and eclipsing in addition to thruster firings. Similar to the magnetic field data preparation, some broadband spurious wave power was observed in the electric field data following spacecraft maneuvers, but that wave power was not noticeable in the azimuthal component of the electric field. Therefore, we inspected the electric field data for charging, eclipsing, and thruster firing events and deleted the orbits when these events occur. Because of the absence of spurious wave power following thruster fires, we only deleted the orbits in which a maneuver occurred without deleting any additional orbits. Removing all three types of events resulted in a further 14% reduction in the data available from RBSP-A and an 11% reduction in the data available from RBSP-B.

Since the E_x component is not provided in the L2 EFW data, we used the EMFISIS fluxgate magnetometer data to compute E_x. The magnetometer data was converted from the SM coordinate system to the mGSE coordinate system; then using the assumption that $\mathbf{E} \cdot \mathbf{B} = 0$, we were able to compute the E_x component. Since small uncertainties in B_x result in large errors in E_x, not all of the values of E_x obtained in this fashion can be used. We started with the given accuracy of the B_x, B_y, B_z, E_y, and E_z measurements and used the standard error propagation formulas to estimate the error in E_x through the transformation of $\mathbf{B}$ from SM coordinates to mGSE coordinates and then through the relation $\mathbf{E} \cdot \mathbf{B} = 0$ [*Squires*, 2001]. After estimating the error in E_x (ΔE_x) we computed the elevation angle that the magnetic field vector forms with the spin plane of the spacecraft in mGSE coordinates,

$$\theta = \left| \arctan\left(\frac{B_x}{\sqrt{B_y^2 + B_z^2}} \right) \right|. \tag{8}$$

We know that a small elevation angle implies a large uncertainty in E_x. Therefore, ΔE_x is a decreasing function of θ. The error ΔE_x decreases very quickly resulting in $\Delta E_x = 0.5$ mV/m when $\theta \approx 5.75°$. Therefore, this is the cutoff we used in our study. All data with an elevation angle $\theta < 5.75°$ were deleted. The electric field data were then converted from mGSE coordinates to SM coordinates, followed by the data's conversion from Cartesian coordinates to polar coordinates giving us the azimuthal component of the electric field E_ϕ, necessary to compute the electric component of the radial diffusion coefficient D_{LL}^E. We would also like to warn the reader here that the EFW L2 data provided does not have a uniform cadence in time. The cadence is slowly changing as a function of time and oscillates around 11 s instead of the reported 12 s. This created two challenges. First, classical Fourier analysis cannot be performed if Δt is not a constant. Second, even if it is erroneously applied to the EFW data assuming that $\Delta t = 12$ s, then the periodogram will be skewed, showing incorrect wave power for a given frequency. Because of this, we resampled E_ϕ to a constant cadence of 12 s before we estimate the power spectral density. E_ϕ was then digitally filtered in exactly the same manner as

the EMFISIS data so that wave power leakage into the ULF range can be avoided. The multitaper technique was then used with 20 min data segments to estimate the power spectral density. The specifications for the digital filter and power spectral density estimation were identical for both the magnetic and the electric field measurements so that the two results may be meaningfully compared and combined.

5. ULF Wave Power Distribution

In order to understand the dependence of ULF wave power on MLT, L^*, and Kp, it is necessary to parameterize the magnetic and electric field power. In MLT, we decided to use four bins of equal size. The MLT bins are centered on 0000 h, 0600 h, 1200 h, and 1800 h with each bin spanning 6 h. The noon bin, for example, spans from 0900 MLT hours to 1500 MLT hours. In L^*, we use six bins which are centered on $L^* = 3$, 3.5, 4, 4.5, 5, and 5.5. Each L^* bin is 0.5 R_E wide. The first bin, for example, spans from $L^* = 2.75$ to $L^* = 3.25$ with the center at $L^* = 3$. In Kp, we are only able to use six bins centered on $Kp = 0$, 1, 2, 3, 4, and 5 because of a dearth of high geomagnetic activity during the Van Allen Probes era. The Kp bins are defined as follows:

$$\begin{aligned} Kp = 0 &\Rightarrow \{0, 0+\}, \quad Kp = 3 \Rightarrow \{3-, 3, 3+\}, \\ Kp = 1 &\Rightarrow \{1-, 1, 1+\}, \quad Kp = 4 \Rightarrow \{4-, 4, 4+\}, \\ Kp = 2 &\Rightarrow \{2-, 2, 2+\}, \quad Kp = 5 \Rightarrow \{5-, 5, 5+, \ldots\}, \end{aligned}$$

where the last bin $Kp = 5$ includes all Kp values larger than 5. Figure 1 shows the number of spectra in various bins after the magnetic field spectra and the electric field spectra have been binned. For a given spectrum, the MLT, L^*, and Kp values assigned to the center of the corresponding data segment determine the bin where that spectrum is assigned. We can see that the statistics degrade as Kp increases. The higher the Kp value, the smaller the amount of data available for both instruments.

Figure 2 shows the magnetic and electric field spectra in the $L^* = 5.5$, $Kp = 2$, noon sector bin. All of the power spectral densities contained in that bin are shown in the background. The plots also show the mean, the geometric mean, and the median power spectral density with the interquartile range. The range of the spectra being several orders of magnitude shows that there can be significant variation even within a single bin. Since the extreme outlying spectra can take on very large values, the mean is a very inadequate measure of central tendency. In Figure 2 we can clearly see that the mean is at the 75th percentile. In such skewed distributions, the geometric mean or the median are much more appropriate as measures of central tendencies. For the ease of calculation and the robustness of the median, we chose the median power spectral density as the representative from each bin to proceed with this study.

Parameterizing the ULF wave power using magnetic local time allows us to study the ULF wave power distribution in azimuth. After selecting the median magnetic and electric spectra from each bin, the spectra are integrated over the truncated frequency range ~0.8 mHz to ~8 mHz giving us the total wave power which can then be readily compared across bins. Figure 3 shows the distribution of total ULF wave power estimates from the magnetic and electric field data. We can see clearly that, in general, the wave power increases as Kp increases, which is to be expected as a higher level of geomagnetic activity results in larger perturbation amplitudes. The ULF wave power varies directly with radial distance as we see an increase in power as L^* increases. In magnetic local time, we see that the noon sector tends to have higher power than the other three sectors with no statistically significant difference in ULF Pc-5 wave power between the dawn, dusk, and midnight sectors. These distributions are similar to the distributions presented in *Ali et al.* [2015] derived from CRRES magnetic field data.

6. Drift-Averaged Spectra and the Radial Diffusion Coefficients

Since the *Fei et al.* [2006] formulation requires the power spectral density of the compressional component of the magnetic field and the azimuthal component of the electric field to be drift averaged, we need to estimate a drift-averaged spectrum. Figure 1 shows us how the bin statistics vary in azimuth for any given L^* and Kp, and hence, taking a weighted average of the spectra seems appropriate here to obtain a drift-averaged power profile. We do not want the measurements in a given local time sector to influence the drift-averaged profile unduly. Therefore, we set the weights to be inversely proportional to the number of measurements in a given MLT sector and for each L^* and Kp obtain a drift-averaged power spectral density for both the magnetic

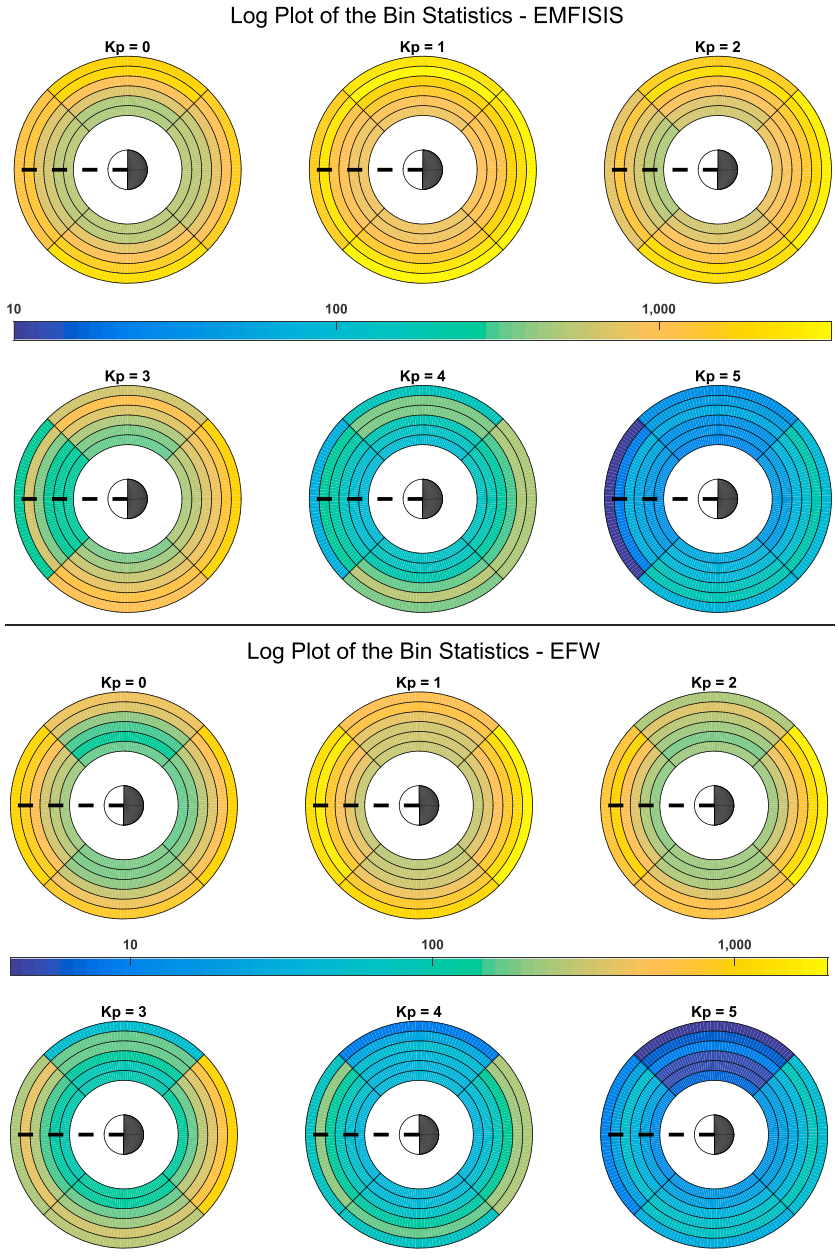

Figure 1. Log plots of the bin statistics for the EMFISIS magnetic field spectra and EFW electric field spectra, separated by *Kp*. The rings correspond to L^* bins between $L^* = 3$ and $L^* = 5.5$ with the dashed line being the Sun-Earth line.

and the electric field measurements. Figure 4 shows the drift-averaged power spectral densities in frequency space, separated by L^* and *Kp* obtained from magnetic and electric fields measurements. In Figure 4, the corresponding energies as well as the relativistically corrected first invariant values are also calculated and shown, assuming the resonance condition in an azimuthally symmetric field configuration $\omega = m\omega_d$ and the azimuthal wave mode number being $m = 1$ for an electron. For the magnetic spectra, we see that for all L^* and *Kp*, the wave power is flat for low frequencies but after about 5 mHz, the wave power decreases in a power law fashion. For the electric field, we see that the spectra are independent of energy under almost all conditions in addition to being independent of L^*. There seems to be a very weak L^* dependence at high frequencies, but at lower frequencies the spectra have little to no L^* dependence.

We used the drift-averaged magnetic and electric field power spectral densities along with the *Fei et al.* [2006] expressions given by equations (5) and (6) to compute the magnetic and the electric components of the radial

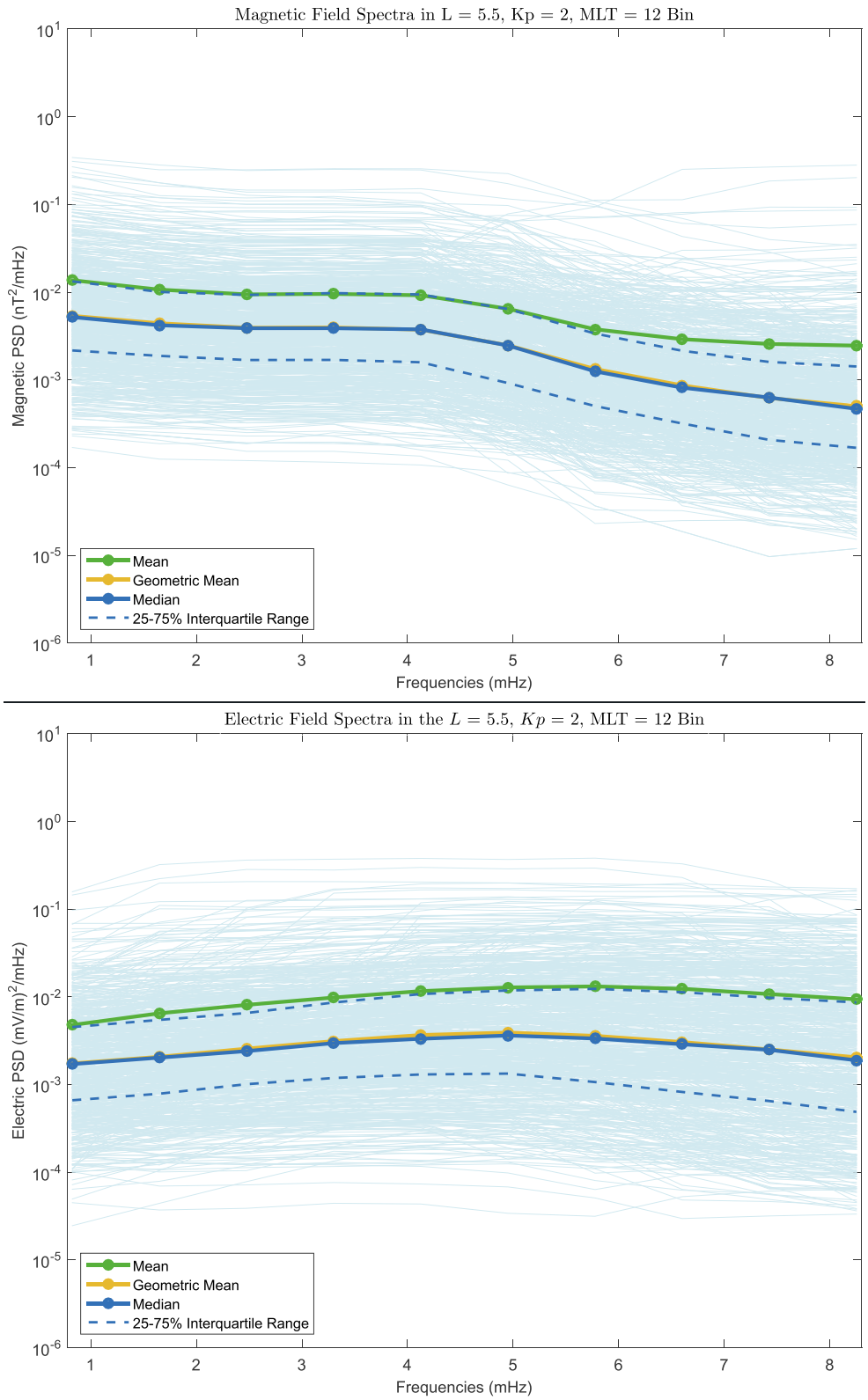

Figure 2. Magnetic and electric field spectra belonging to the L^* = 5.5, Kp = 2, noon sector bin with the mean, geometric mean, and the median PSD.

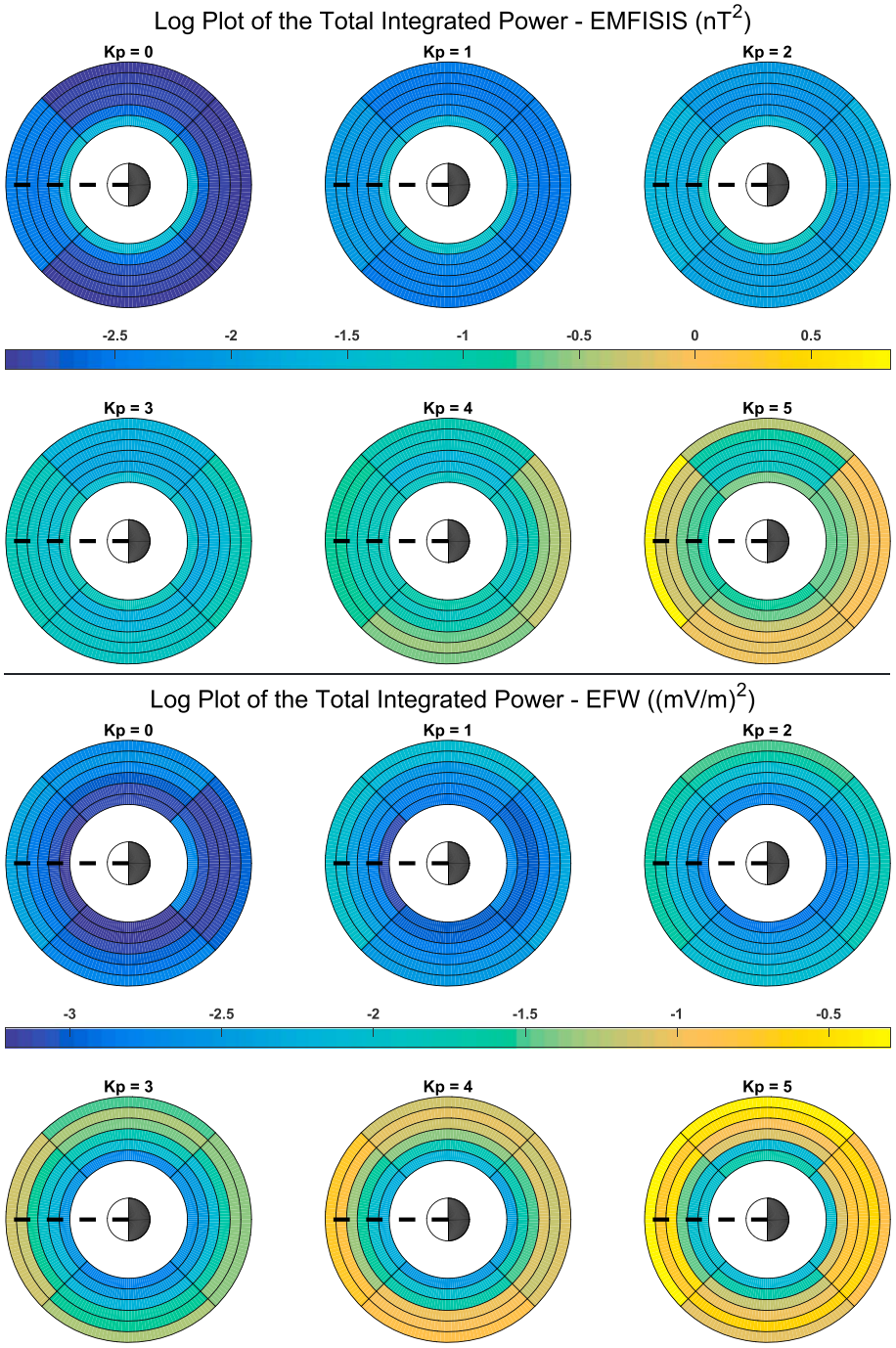

Figure 3. Distribution of the total ULF wave power from the magnetic and electric field measurements integrated from ~0.8 mHz to ~8 mHz. The dashed line is the Sun-Earth line.

diffusion coefficient, D_{LL}^{B}[RBSP] and D_{LL}^{E}[RBSP]. Figure 5 shows the magnetic and the electric components of the radial diffusion coefficient as a function of frequency separated by L^* and *Kp*. For the magnetic component, there is a clear energy dependence, with the magnetic component, at low energies, increasing with increasing energy. After a very weak maximum at about 4 mHz, the magnetic component then decreases very slowly as energy continues to increase. One thing to note about the electric component is that it is independent of energy for all L^* and *Kp*. The electric diffusion rates are flat most of the time, with the energy dependence being very minute and negligible when it does occur at high energies. A second thing to note is that the electric component is much larger than the magnetic component, sometimes by 2 orders of magnitude.

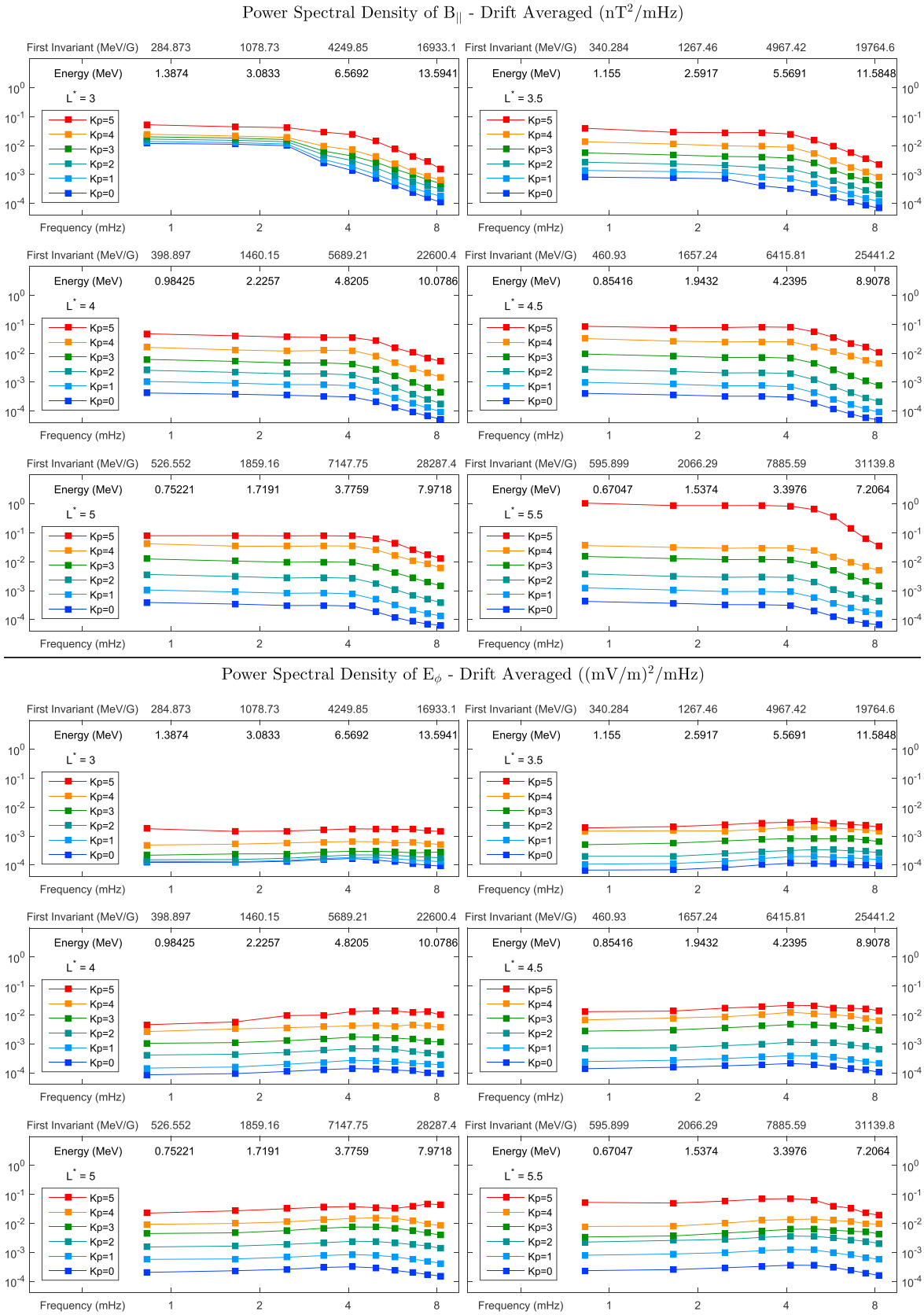

Figure 4. Drift-averaged spectra from the magnetic and electric field measurements as a function of electron drift frequency separated by L^* and *Kp*. The electron energies and relativistically corrected first invariant values are computed assuming $\omega = \omega_d$.

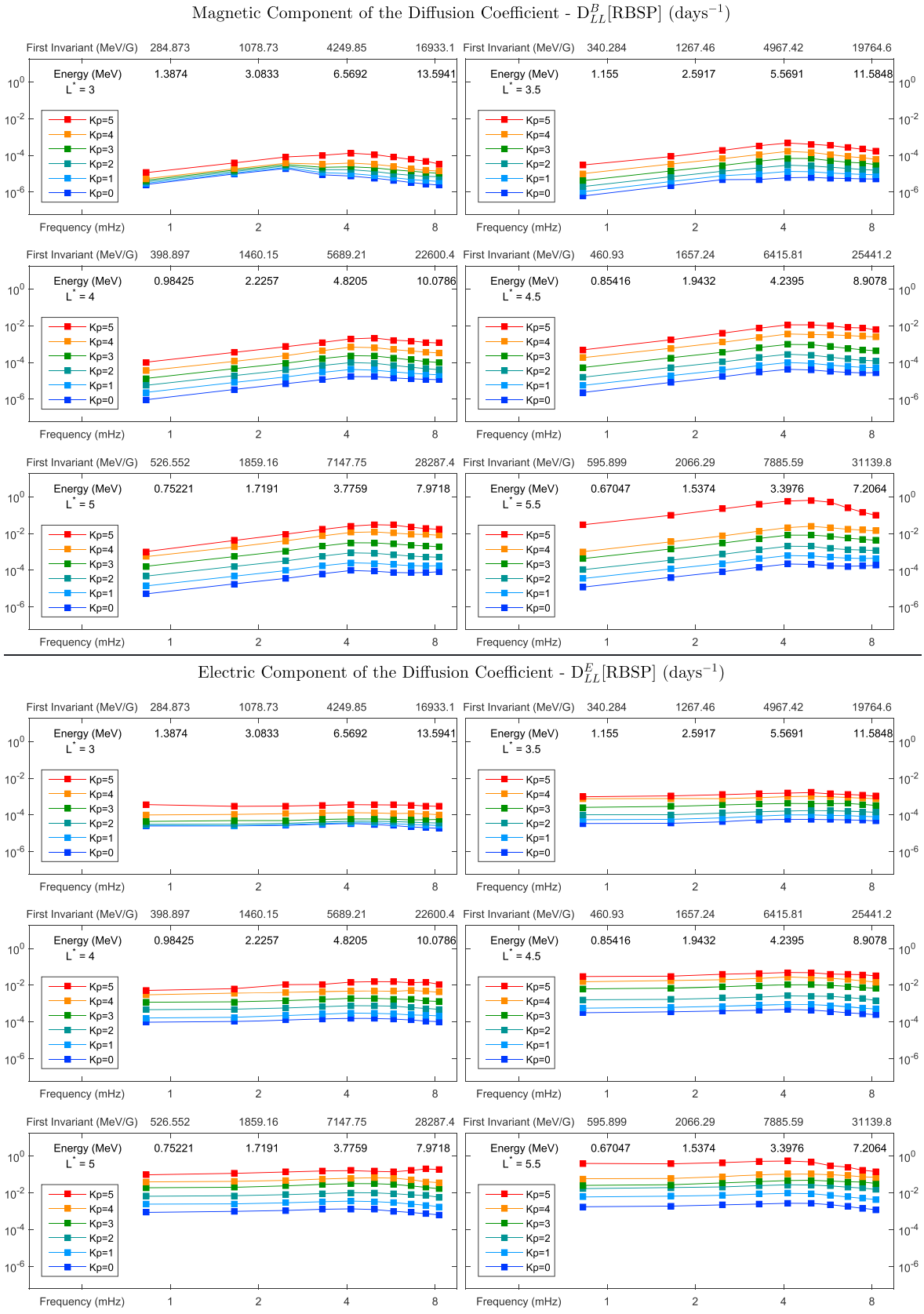

Figure 5. The magnetic and electric components of the radial diffusion coefficient in frequency space separated by L^* and *Kp*.

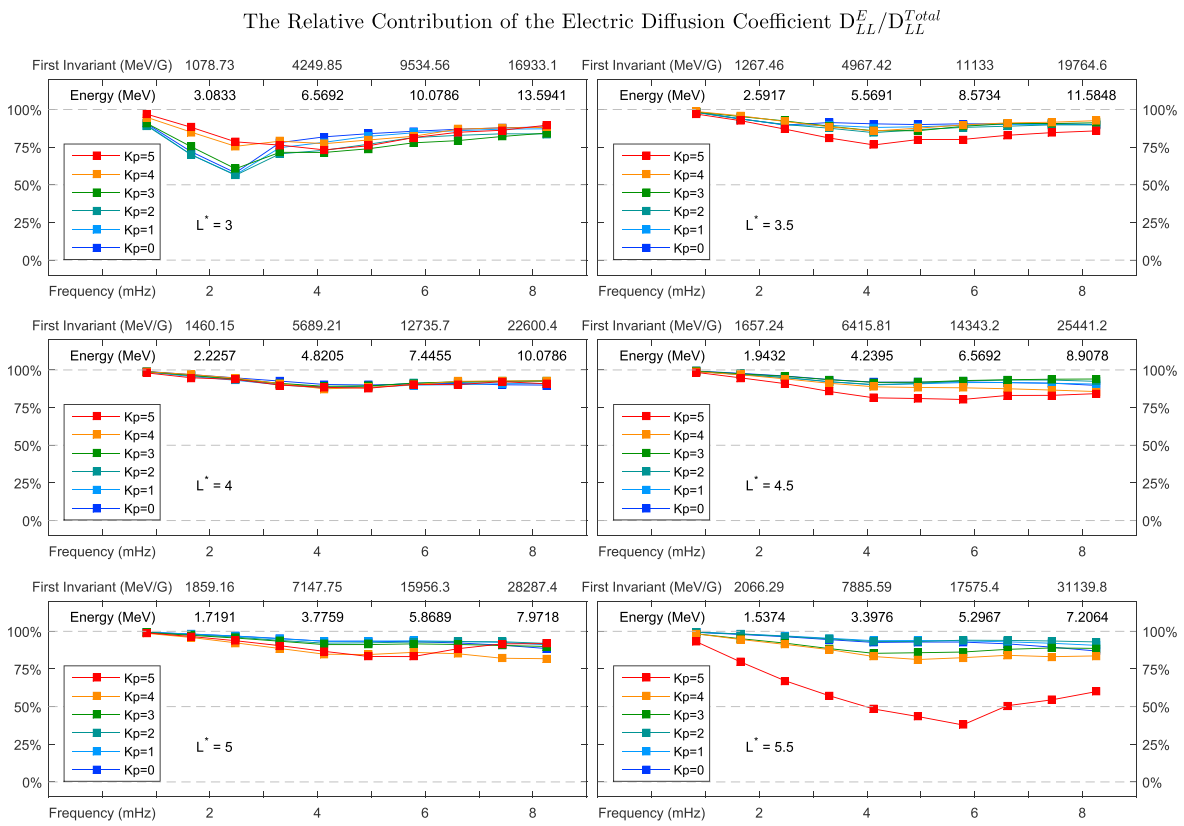

Figure 6. The relative contribution of the electric component of the diffusion coefficient to the total diffusion rate. It is clear that the electric field perturbations are almost always dominant in driving radial diffusion.

Figure 6 quantifies the relative contribution of the electric component to driving radial diffusion of charged particles. Figure 6 shows the quantity $100\% \cdot (D_{LL}^{E}/D_{LL}^{\mathrm{Total}})$ as a function of energy separated by L^* and Kp. We can see that the electric component contributes significantly more to radial diffusion than does the magnetic component. The contribution of the electric component can be as high as 99%, which implies that the electric component is 2 orders of magnitude larger than the magnetic component. The only exception is the $L^* = 5.5$ case for $Kp = 5$. We must remind the reader here that for $Kp = 5$, the statistics are very poor, especially for the electric field measurements (as can be seen in Figure 1). Thus, the implication that the magnetic field perturbations are dominant or just as important as the electric field perturbations for high Kp at high L^* may very well be false. Therefore, we submit here that, in general, the electric component is dominant over the magnetic component in driving radial diffusion of charged particles inside the given energy ranges. Both of the components should be considered when radial diffusion is used to model the Van Allen radiation belts. Considering Figure 6, if one of the components is to be ignored, then it should be the magnetic component D_{LL}^{B}. The magnetic component contributes very little most of the time, and the approximation

$$D_{LL}^{\mathrm{Total}}[\mathrm{RBSP}] \approx D_{LL}^{E}[\mathrm{RBSP}]$$

may be used if an approximation is desired by the modeling community. We would also like to clarify here that since the magnetic component is relatively inconsequential in driving radial diffusion, the total radial diffusion coefficient plots are almost identical to the electric radial diffusion plots. For this reason, with the exception of Figure 9, we present no figures showing the total radial diffusion coefficients. If, for example, the reader wishes to see $D_{LL}^{\mathrm{Total}}[\mathrm{RBSP}]$ as a function of L^* for a fixed first invariant, then the reader is referred to the bottom panel of Figure 7. The curves for $D_{LL}^{E}[\mathrm{RBSP}]$ are nearly identical to the curves for $D_{LL}^{\mathrm{Total}}[\mathrm{RBSP}]$.

In addition, even though *Fei et al.* [2006] assumed no phase relation between the magnetic field and the induced electric field, *Perry et al.* [2005, Figure 1] shows clearly that E_ϕ and $\partial B_\theta/\partial t$ have negatively correlated phases when E_ϕ and B_θ are derived from an azimuthal vector potential component which models the inductive electric of a poloidal mode ULF wave. This results in a decrease in the electric component of the

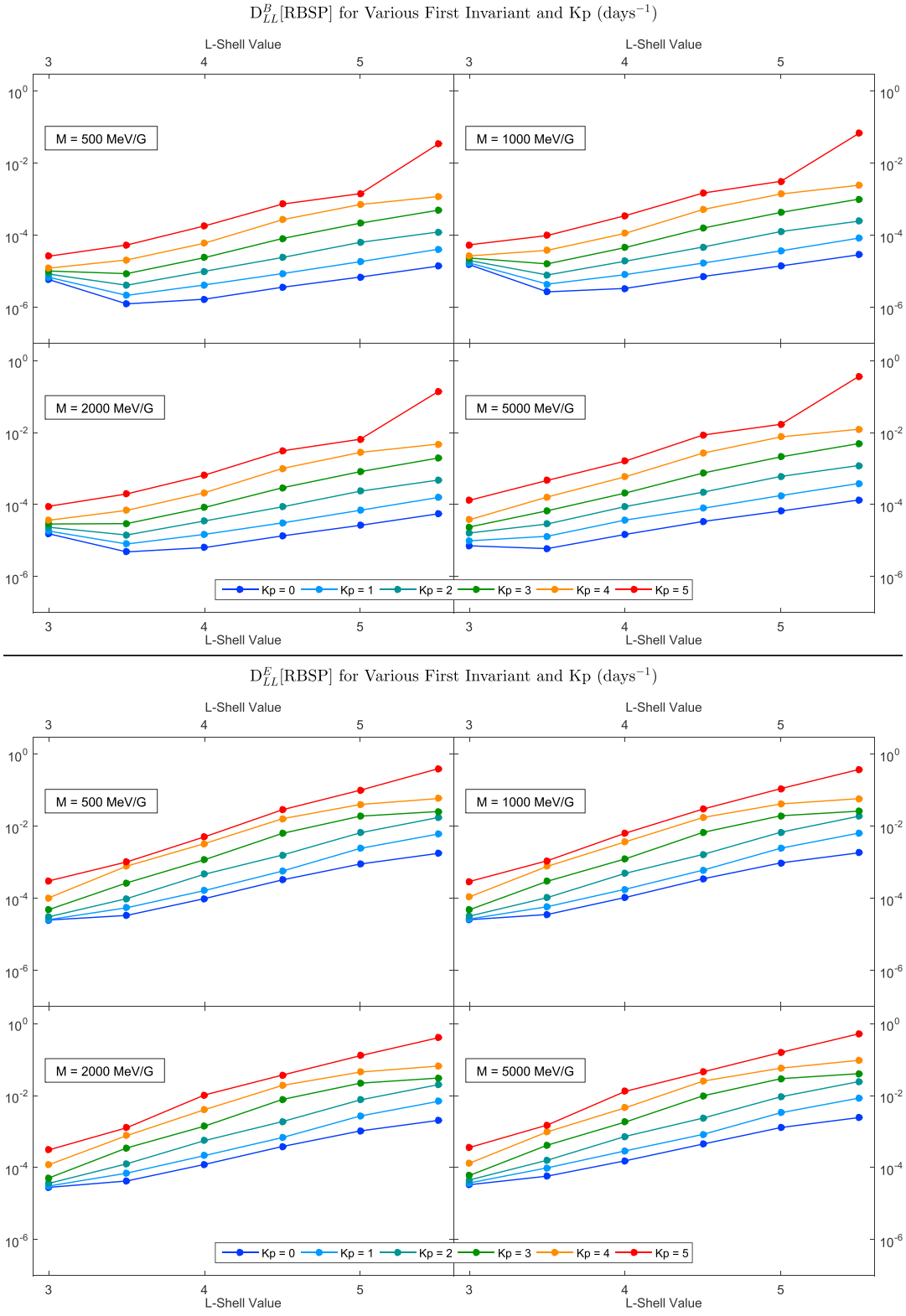

Figure 7. The magnetic and electric components of the radial diffusion coefficient for various constant values of the first invariant *M* as a function of L^* separated by *Kp*.

radial diffusion coefficient by about a factor of 2. While this may affect the magnitude of the electric component, this does not alter the main conclusion of this paper that the perturbations in the electric field dominate in driving radial diffusion.

The drift frequency f varies directly with M and inversely with L^2 as given by

$$f = \frac{3M}{2\pi\gamma q L^2 R_E^2}, \tag{9}$$

$$\gamma = \left[1 + \frac{2BM}{m_0 c^2}\right]^{1/2}, \tag{10}$$

$$= 1 + \frac{W}{W_{\text{rest}}}, \tag{11}$$

$$W = W_{\text{rest}}(\gamma - 1), \tag{12}$$

$$= W_{\text{rest}}\left[\left(1 + \frac{2BM}{m_0 c^2}\right)^{1/2} - 1\right], \tag{13}$$

where we assume SI units and a symmetric dipole field resulting in the factor of 2π in the expression for f. For any other magnetic field model, the factor 2π must be replaced by integrating the period function over one complete drift orbit. Here M is the relativistically correct first invariant, γ is the relativistic correction factor, q is the charge of the particle, R_E is the Earth's radius, W_{rest} is the rest energy of the particle, and B is the strength of the local magnetic field which assumes a symmetric dipole field, approximated by B_0/L^3 where B_0 is the strength of the magnetic field on the surface of the Earth. Since we have two algebraic equations relating four variables; L, the first invariant M, frequency f, and energy W, we have 2 degrees of freedom in this algebraic system. This means that given the values of any two of the variables it is very straightforward to compute the other two variables.

As Figure 7 shows, D_{LL}^{B}[RBSP] and D_{LL}^{E}[RBSP] span several orders of magnitude as a function of L^* even for a fixed M or Kp. For a given component, magnetic or electric, obtaining a global model which approximates the component with reasonable accuracy is difficult. Determining a relatively simple model, which would be a function of L^*, M, and Kp while capturing most of the variation of the given component, is considerably more difficult. Therefore, in order to obtain a simple model for each component, we used a genetic algorithm with the fitness function being the sum of the residuals squared in the least squares sense [*Coley*, 1999]. Numerous runs of the algorithm resulted in numerous models which were then sorted and ranked according to the complexity of the model. The complexity of a model can be gauged by counting the number of terms presented in the model, how many operations are required to evaluate the model, and how complex the individual terms are in the model. For example, a monomial term is simpler than a term involving a hyperbolic function. After we selected a reasonably simple model, we performed weighted least squares for each component and obtained

$$D_{LL}^{B}[\text{RBSP}] = \exp\left(a_1 + b_1 \cdot Kp \cdot L^* + L^*\right), \tag{14}$$

$$D_{LL}^{E}[\text{RBSP}] = \exp\left(a_2 + b_2 \cdot Kp \cdot L^* + c_2 \cdot L^*\right), \tag{15}$$

where the constants are given by

$$a_1 = -16.253,\ b_1 = 0.224,$$
$$a_2 = -16.951,\ b_2 = 0.181,\ c_2 = 1.982,$$

with L^* and Kp being unitless parameters. Both D_{LL}^{B}[RBSP] and D_{LL}^{E}[RBSP] components are returned in units of days^{-1}.

We would like to emphasize here that neither of these models has any physical basis, and they are presented solely as compact representations of the estimated diffusion coefficients in order to aid the community with its modeling efforts. These models are much more succinct and easier to use than large tables containing numerical values of D_{LL}^{B} and D_{LL}^{E} or dozens of fitted curves. The domain used while fitting both of these models was $3.0 \le L^* \le 5.5$ and $0 \le Kp \le 5$. The data used to fit both models corresponded to M between 500 MeV/G

Table 1. Scaling Exponents, as the Magnetic and the Electric Components Are Fit to a Simple Power Law as a Function of L^*, Separated by *Kp*

	Level of Geomagnetic Activity (*Kp*)					
	0	1	2	3	4	5
D_{LL}^{B}[RBSP]	5.41	6.50	7.82	9.28	9.23	8.90
D_{LL}^{E}[RBSP]	7.67	9.13	10.66	10.91	10.87	11.58

and 5000 MeV/G. Since both components exhibited a very weak energy dependence, models returned by the genetic algorithm reflected this fact. If a model contained an energy term, then the coefficient of that term would be small and the term would explain very little of the variance in the data. The increase in the complexity of the model by including an energy term was certainly not worth the negligible reduction in error it provided. Therefore, for both components, we present models without an *M* dependence.

Both models provide excellent results not only for interpolation inside the domain but also for extrapolation outside the domain since the models are continuous in both L^* and *Kp*. *Kp* can take any value in $\{0, 0.3, 0.7, 1, ..., 4.3, 4.7, 5\}$ while L^* can vary continuously for $3.0 \leq L^* \leq 5.5$. Furthermore, the trends inside the domain for both parameters continue in a reasonable manner outside of the domain. For *Kp*, it is possible to plug in any value in $\{0, 0.3, 0.7, 1, 1.3, ..., 8.3, 8.7, 9\}$ while the limits on L^* are left to the individual reader to decide. A similar warning holds for the parameter *M*. These models assume that for *M* between 500 MeV/G and 5000 MeV/G, the data exhibit a very weak *M* dependence. It is left up to the individual reader to decide how far outside the *M* domain this assumption holds true. Obviously, if we move far enough away from the boundary of the domain, the diffusion coefficients simply become unreliable. The reader has the option of just using the nearest neighbor approximation for points outside of the domain. For example, value of $Kp = 5$ can be used for all $Kp > 5$, $L^* = 3.0$ can be used for lower L^* shell values, and so on.

Early research efforts [*Fälthammar*, 1965, 1966a, 1966b, 1968; *Cornwall*, 1968; *Birmingham*, 1969] to estimate the radial diffusion coefficients using magnetic and electric field models resulted in an L^6 dependence of the radial diffusion coefficient. *Fälthammar* [1968] also presented the electromagnetic diffusion coefficient D_{LL}^{M} proportional to L^{10} for particles with nonrelativistic energies in a dipole magnetic field including the contributions from the induced electric field. Therefore, investigating the *L* dependence of empirically derived diffusion coefficients is interesting in its own right. Considering Figure 7, both components of the diffusion coefficients have a linear trend with respect to L^* in log-log space, but the scaling exponent seems to depend on the level of geomagnetic activity. Therefore, we fit both components of the diffusion coefficients as functions of L^* to a simple power law $D_{LL} = D_0 L^n$ separated by *Kp*. The scaling exponents *n* are given in Table 1, where we see that the estimates of the scaling exponent *n* are *Kp* dependent and generally increase as *Kp* increases. Since we assumed the diffusion coefficients to be independent of *M*, the scaling exponents are also a constant as a function of *M*. This is in contrast with the *Ozeke et al.* [2012] and *Ozeke et al.* [2014] conclusions that the magnetic coefficients decrease noticeably as *M* increases.

There are many previously published estimates of diffusion coefficients, but due to differences in models and observations used for diffusion coefficient calculations, a comprehensive comparison is difficult. Difference in methodologies as well as in parameters chosen to parameterize diffusion coefficients may make such comparisons of little value. *Brautigam and Albert* [2000] started with the assumption that the root-mean-square of the electric field amplitude is a linear function of *Kp* and then used *Cornwall* [1968] expressions to estimate D_{LL}^{E} using *L*, *M*, and *Kp* as parameters. *Elkington et al.* [2003] used a compressed dipole field with analytic expressions to drive a test particle simulation at geosynchronous distance. *Brautigam et al.* [2005] assumed a purely dipole field and used the electric field measurements from CRRES to numerically estimate D_{LL}^{E} using *L* and *Kp* as parameters. *Fei et al.* [2006] used a compressed dipole field with analytic expressions to solve the diffusion equation between $2 \leq L \leq 10$ and computed D_{LL}^{B} assuming a static *L* dependence with the scaling exponent being 8.5. *Huang et al.* [2010b] used Lyon-Fedder-Mobarry (LFM) model runs to conduct particle simulations and estimate D_{LL}^{B}. *Ozeke et al.* [2012] and *Ozeke et al.* [2014] used in situ measurements from both AMPTE and GOES to compute D_{LL}^{B} along with ground magnetic field measurements mapped to electric field PSDs in space to compute D_{LL}^{E}. *Tu et al.* [2012] used LFM MHD simulations and observations from GOES and THEMIS to estimate both D_{LL}^{B} and D_{LL}^{E}. *Ali et al.* [2015] used the CRRES magnetometer data to estimate D_{LL}^{B} as a function of *L* and *Kp* in direct comparison with the *Brautigam et al.* [2005] study. *Liu et al.* [2016] used 7 years of electric field

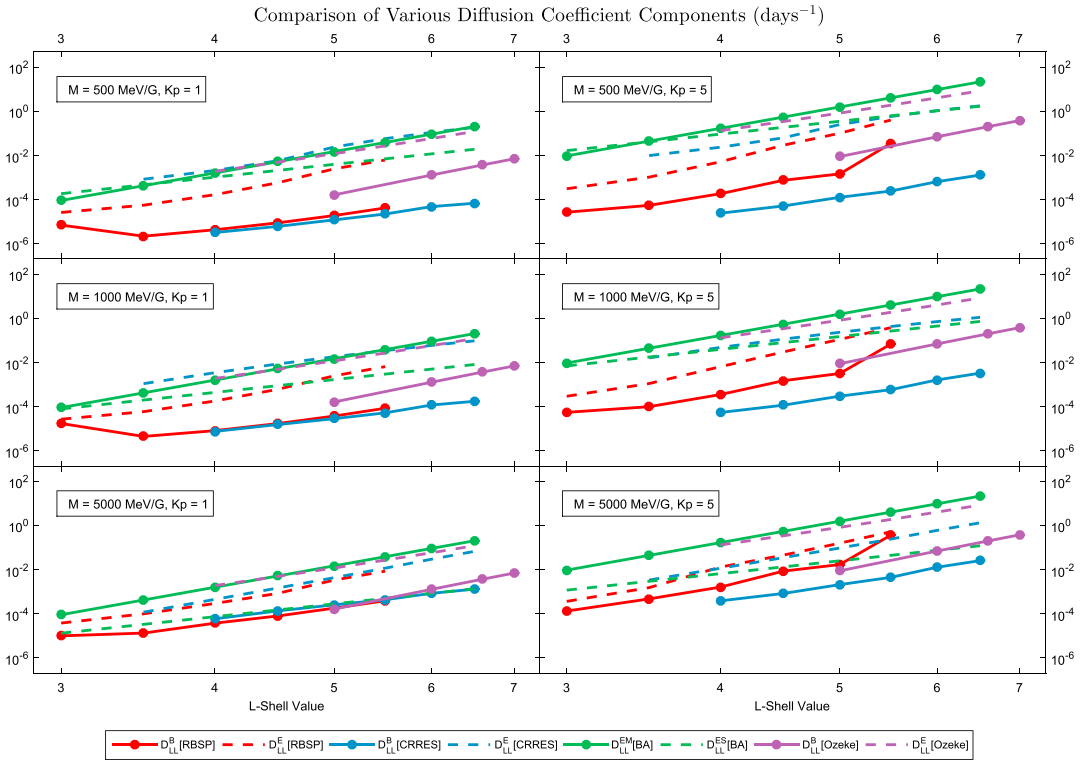

Figure 8. A comparison of various radial diffusion rates. D_{LL}^{B}[RBSP] and D_{LL}^{E}[RBSP] are presented here with D_{LL}^{B}[CRRES] from *Ali et al.* [2015] and D_{LL}^{E}[CRRES] from *Brautigam et al.* [2005] in addition to *Brautigam and Albert* [2000] and *Ozeke et al.* [2012, 2014] estimates.

measurements from THEMIS-D to calculate the D_{LL}^{E}[THEMIS], which is consistently higher than D_{LL}^{E}[CRRES] in magnitude. D_{LL}^{E}[THEMIS] also shows considerable deviation from the D_{LL}^{E}[CRRES] and the D_{LL}^{M}[BA] estimates with the deviation increasing as *Kp* increases.

Since *Kp* is a common index of activity used in previous diffusion rate studies, we chose *Kp* as our activity-dependent parameter. Unfortunately, there has been a dearth of high geomagnetic activity during the Van Allen Probes era to date and there are virtually no measurements for *Kp* higher than 5 which could be useful to us for this study. Figure 8 shows the comparison of our electric and magnetic components of radial diffusion coefficients with some of the previously published estimates. D_{LL}^{B}[RBSP] and D_{LL}^{E}[RBSP] are the diffusion coefficients computed using the Van Allen Probes magnetic and electric field measurements. D_{LL}^{B}[CRRES] were presented in *Ali et al.* [2015] and were computed using the CRRES fluxgate magnetometer data with techniques very similar to the current Van Allen Probes study. D_{LL}^{E}[CRRES] estimates are taken from *Brautigam et al.* [2005] which used the electric field measurements from CRRES. We point out here that although *Brautigam et al.* [2005] used the *Fälthammar* [1965] diffusion formulation, they made no effort to separate the inductive and the convective component of the electric field measurements since it is quite difficult to do so with single-point measurements from a spacecraft such as CRRES. Therefore, D_{LL}^{E}[CRRES] contains contributions from the total electric field. D_{LL}^{EM}[BA] and D_{LL}^{ES}[BA] are the electromagnetic and electrostatic components from *Brautigam and Albert* [2000]. D_{LL}^{B}[Ozeke] and D_{LL}^{E}[Ozeke] are taken from *Ozeke et al.* [2012] and *Ozeke et al.* [2014].

Figure 9 shows the total diffusion coefficients obtained by adding up the two individual components. The D_{LL}^{Total}[RBSP] and D_{LL}^{Total}[BA] diffusion components can just be added as they are, because both components have identical *L* domains. There is no extrapolation or truncation needed to match the *L* domains. For D_{LL}^{Total}[CRRES], the electric component had to be truncated to $4 \leq L \leq 6.5$ before the magnetic component could be added to it. For D_{LL}^{Total}[Ozeke], the magnetic component had to be interpolated and truncated while the electric component had to be truncated so that the total diffusion coefficient can be obtained for $5 \leq L \leq 6.5$. The total diffusion coefficient is perhaps better for comparison between different estimates

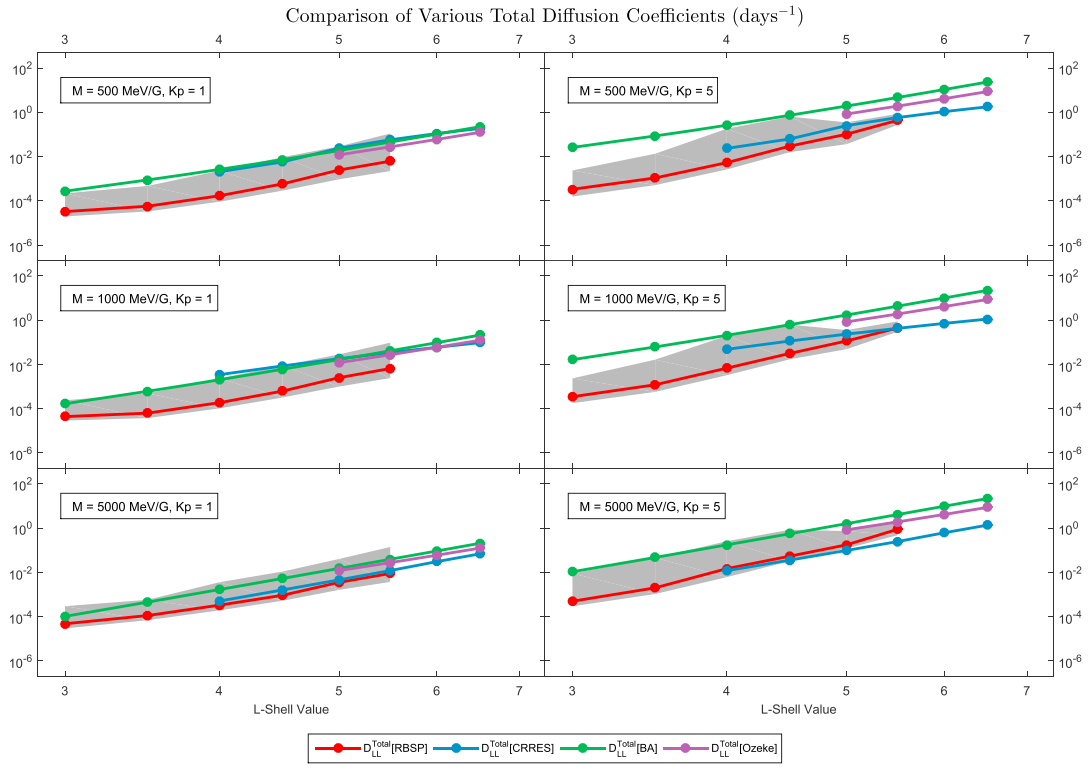

Figure 9. A comparison of various total radial diffusion rates. The shaded area represents the 5th and the 95th percentile for the D_{LL}^{Total}[RBSP] estimates.

because of the different formulations used. The *Fälthammar* [1965, 1966a, 1966b, 1968] formulation divides the total radial diffusion coefficient into the electrostatic and the electromagnetic component, while the *Fei et al.* [2006] formulation partitions it into the magnetic and the electric component. Since the electromagnetic component contains contributions from the magnetic field as well as the inductive electric field, the electromagnetic component will tend to be larger than the purely magnetic component and the electrostatic component will tend to be smaller than the total electric component. Adding up the components before comparison alleviates this problem. The total diffusion coefficient includes contributions from the magnetic field, convective electric field, and the inductive electric field once and only once. Hence, the comparison becomes more meaningful.

The shaded region in Figure 9 represents the uncertainty in the D_{LL}^{Total}[RBSP] estimates. In Figure 2, where we presented all of the magnetic and electric field spectra in a given bin, we see that the range of the spectra can be 3 to 4 orders of magnitude even if particular values of L^* and Kp are fixed. We picked the median power spectral density as an appropriate indicator of central tendency but it is also important to note the large degree of variability present in each bin. Therefore, in addition to the median, we took the data at the 5th and the 95th percentile from each bin and estimated the upper bounds and the lower bounds on both the D_{LL}^{B}[RBSP] and D_{LL}^{E}[RBSP] estimates. These bounds on both of the components were then combined to estimate the uncertainty in $D_{LL}^{Total[RBSP]}$. The uncertainty was estimated at each step of calculation using standard error propagation formulas [*Squires*, 2001].

The distribution of the spectra within a bin appears to be a lognormal distribution although we cannot verify this in a statistically significant way. Attempts to use a statistical test to determine if the spectra are distributed lognormally resulted in rejection of the null hypothesis in about half of the cases, and we therefore could not make a quantitative statement in general about all of the bins. Some of the bins are clearly deficient because there are not enough spectra in them to guess their probability distribution function. But for most bins, the distribution in log space appears to be symmetric and bell shaped. This implies that in linear space the mass of the distribution is concentrated on the left, near zero, with very small magnitudes, which is indeed the case. The tail on the right is long, containing some spectra with extremely large magnitudes. This results in

the 5th percentile being very close to the median while the 95th percentile can be an order of magnitude larger than the median. The effect clearly propagates all the way to Figure 9, where we see the upper limit on D_{LL}^{Total}[RBSP] being rather large while the lower limit is barely visible. We point out here that all of the data processing and the statistical analysis presented in this paper were done in linear space. The data are only plotted in log space, when necessary, to make some of the relationships clear. Therefore, in Figure 2, the mean, the geometric mean, and the median with the interquartile range were computed in linear space, which is why the mean is at the 75th percentile. This is precisely the reason why we chose the median as the measure of central tendency instead of the arithmetic mean. The arithmetic mean is a very inadequate measure of the location for this distribution.

Comparing our estimates with other previously published results in Figure 8, we see that for quiet times the magnetic components from Van Allen Probes, CRRES, and *Ozeke et al.* [2012, 2014] are in good agreement, with the agreement getting better as energy increases. For higher *Kp*, the agreement between Van Allen Probes and *Ozeke et al.* [2012, 2014] is better than with CRRES. One trend which we see in general is that the magnetic component is always smaller than the electric component lending credence to the fact that the perturbations in the electric field are more important than the perturbations in the magnetic field in driving radial diffusion of charged particles in the inner magnetosphere. This has important consequences for Van Allen radiation belt modelers [*Shprits et al.*, 2005; *Varotsou et al.*, 2008; *Albert et al.*, 2009; *Tu et al.*, 2009; *Chu et al.*, 2010; *Su et al.*, 2010, 2011a, 2011b; *Subbotin et al.*, 2011a, 2011b; *Kim et al.*, 2012; *Tu et al.*, 2013; *Li et al.*, 2014; *Zheng et al.*, 2014] who assume that the magnetic diffusion coefficients are much larger than the electric diffusion coefficients. Recent efforts by *Ozeke et al.* [2012, 2014], *Ali et al.* [2015], and *Liu et al.* [2016] along with the present study suggest that the reverse is true. The electric diffusion coefficient is dominant in driving radial diffusion sometimes by 2 orders of magnitude. Comparing the total diffusion coefficients from Figure 9, we see that D_{LL}^{Total}[RBSP] is consistently smaller than the *Brautigam and Albert* [2000] estimates. For lower energies and for quiet times, the D_{LL}^{Total}[CRRES] and D_{LL}^{Total}[Ozeke] estimates agree quite well with the *Brautigam and Albert* [2000] estimates. But as energy and the level of geomagnetic activity increase, the D_{LL}^{Total}[CRRES] and D_{LL}^{Total}[Ozeke] estimates approach the D_{LL}^{Total}[RBSP] estimates. Note that the D_{LL}^{Total}[CRRES] and the D_{LL}^{Total}[Ozeke] estimates are always within the D_{LL}^{Total}[RBSP] error bounds albeit being at the upper boundary occasionally. On the other hand, the difference between D_{LL}^{Total}[RBSP] and D_{LL}^{Total}[BA] is simply too large at times, and the *Brautigam and Albert* [2000] estimates are not within the error estimates of D_{LL}^{Total}[RBSP].

7. Summary and Discussion

It has long been established that stochastic perturbations in both the magnetic and the electric fields may contribute to driving radial diffusion of charged particles in Earth's inner magnetosphere [*Fälthammar*, 1965, 1966a, 1966b, 1968]. Therefore, it is important for modelers to understand the relationship between the two components qualitatively and quantitatively. This will assist us in understanding how various physical processes such as pitch angle, energy, and radial diffusion along with convective transport, couple and contribute to the buildup and depletion of the Van Allen radiation belts. We used the magnetic and electric field measurements from EMFISIS and EFW instruments (respectively) on board the Van Allen Probes to compute the compressional component of the magnetic field and the azimuthal component of the electric field. The power spectral densities of both components were parameterized as functions of the Roederer L^* [*Roederer and Zhang*, 2014], *Kp*, and magnetic local time. In MLT, we saw that the noon sector generally contains more ULF Pc-5 wave power than other MLT sectors with there being no statistically significant difference among the other MLT sectors. ULF wave power is not uniform in azimuth (as seen in Figure 3) but all analytic treatments of radial diffusion assume constant ULF wave power in azimuth. Clearly, this issue deserves more attention from the space physics community.

The MLT-dependent spectra were then used to derive drift-averaged spectra as function of L^* and *Kp* which were then used with the *Fei et al.* [2006] formulation to obtain the magnetic and the electric components of the radial diffusion coefficients (D_{LL}^{B}[RBSP] and D_{LL}^{E}[RBSP]). In order to use the *Fei et al.* [2006] formulation, we assumed that the first wave mode number $m = 1$ contains all of the observed magnetic and electric field wave power. This assumption was made explicitly in *Ali et al.* [2015] and *Brautigam et al.* [2005] and is necessary because it is difficult to gauge the distribution of wave power across wave mode numbers with only single-point measurements such as those from CRRES or from the Van Allen Probes. In order to study wave power distribution in the first m modes, we need at least $2m$ independent measurements simultaneously

in time. The magnetic component of the diffusion coefficient has an energy dependence although it is not very strong. The electric component has such a weak energy dependence that for numerical modeling purposes we can assume that the electric component is independent of energy. Furthermore, we confirm that the electric component is dominant, over the magnetic component, in driving radial diffusion, sometimes by as much as 2 orders of magnitude. This should be considered carefully when modelers design simulations to understand the dynamic evolution of the radiation belts.

Acknowledgments
The electric field measurements were obtained from the EFW instrument data repository located at http://www.space.umn.edu/rbspefw-data/. The magnetic field measurements were obtained from the EMFISIS instrument data repository located at http://emfisis.physics.uiowa.edu/data/index. The ephemeris data are available as an RBSP-ECT data service provided by the Los Alamos National Laboratory at http://www.rbsp-ect.lanl.gov/science/DataDirectories.php. This work was supported by the NASA grants NNX15AF59G, NNX14AC04G, NNX13AE39G, NNX15AI93G, and NNx14AN55G and the NASA Earth and Space Science Fellowship (NESSF) grant NNX13AO43H. Authors Ashar Ali and Scot Elkington would like to thank Louis Ozeke, Yuri Shprits, and Mary Hudson for their valuable remarks which aided this study. Ashar Ali would like to thank Alexander Drozdov, Ksenia Orlova, and Kyle Murphy for many helpful discussions.

References

Albert, J. M., N. P. Meredith, and R. B. Horne (2009), Three-dimensional diffusion simulation of outer radiation belt electrons during the 9 October 1990 magnetic storm, *J. Geophys. Res.*, *114*(A09214), doi:10.1029/2009JA014336.

Ali, A. F., S. R. Elkington, W. Tu, L. G. Ozeke, A. A. Chan, and R. H. W. Friedel (2015), Magnetic field power spectra and magnetic radial diffusion coefficients using CRRES magnetometer data, *J. Geophys. Rev. Space Physics*, *120*, 973–995, doi:10.1002/2014JA020419.

Arthur, C. W., R. L. McPherron, L. J. Lanzerotti, and D. C. Webb (1978), Geomagnetic field fluctuations at synchronous orbit: 1. Power spectra, *J. Geophys. Res.*, *83*, 3859–3865, doi:10.1029/JA083iA08p03859.

Baker, D. N. (2001), Satellite anomalies due to space storms, in *Space Storms and Space Weather Hazards, NATO Sci. Ser.*, vol. 38, edited by I. A. Daglis, pp. 285–311, Kluwer Acad., Dordrecht, Netherlands., doi:10.1007/978-94-010-0983-6_11

Baumjohann, W., and R. A. Treumann (1997), *Basic Space Plasma Physics*, Imperial College Press, London.

Birmingham, T. J. (1969), Convection electric fields and the diffusion of trapped magnetospheric radiation, *J. Geophys. Res.*, *74*(9), 2169–2181, doi:10.1029/JA074i009p02169.

Brautigam, D. H., and J. M. Albert (2000), Radial diffusion analysis of outer radiation belt electrons during the October 9, 1990 magnetic storm, *J. Geophys. Res.*, *105*(A1), 291–309, doi:10.1029/1999JA900344.

Brautigam, D. H., G. P. Ginet, J. M. Albert, J. R. Wygant, D. R. Rowl, A. Ling, and J. Bass (2005), CRRES electric field power spectra and radial diffusion coefficients, *J. Geophys. Res.*, *110*, A02214, doi:10.1029/2004JA010612.

Cahill, L. J., and J. R. Winckler (1992), Periodic magnetopause oscillations observed with the GOES satellites on March 24, 1991, *J. Geophys. Res.*, *97*(A6), 8239–8243, doi:10.1029/92JA00433.

Chen, L., and A. Hasegawa (1991), Kinetic theory of geomagnetic pulsations: 1. Internal excitations by energetic particles, *J. Geophys. Res.*, *96*(A2), 1503–1512, doi:10.1029/90JA02346.

Chu, F., M. K. Hudson, P. Haines, and Y. Shprits (2010), Dynamic modeling of radiation belt electrons by radial diffusion simulation for a 2 month interval following the 24 March 1991 storm injection, *J. Geophys. Res.*, *115*, A03210, doi:10.1029/2009JA014409.

Claudepierre, S. G., S. R. Elkington, and M. Wiltberger (2008), Solar wind driving of magnetospheric ULF waves: Pulsations driven by velocity shear at the magnetopause, *J. Geophys. Res.*, *113*, A05218, doi:10.1029/2007JA012890.

Claudepierre, S. G., M. Wiltberger, S. R. Elkington, W. Lotko, and M. K. Hudson (2009), Magnetospheric cavity modes driven by solar wind dynamic pressure fluctuations, *Geophys. Res. Lett.*, *36*, L13101, doi:10.1029/2009GL039045.

Coley, D. A. (1999), *An Introduction to Genetic Algorithms for Scientists and Engineers*, World Sci., Singapore.

Cornwall, J. M. (1968), Diffusion processes influenced by conjugate-point wave phenomena, *Radio Sci.*, *3*(7), 740–744.

Cravens, T. E. (2004), *Physics of Solar System Plasmas, Cambridge Atmospheric and Space Science Series*, Cambridge Univ. Press, New York.

Elkington, S. R. (2006), A review of ULF interactions with radiation belt electrons, in *Magnetospheric ULF Waves: Synthesis and New Directions, Geophys. Monogr. Ser.*, vol. 169, edited by K. Takahashi et al., pp. 177–193, AGU, Washington, D. C.

Elkington, S. R., M. K. Hudson, and A. Chan (1999), Acceleration of relativistic electrons via drift-resonant interaction with toroidal-mode Pc-5 ULF oscillations, *Geophys. Res. Lett.*, *26*(21), 3273–3276, doi:10.1029/1999GL003659.

Elkington, S. R., M. K. Hudson, and A. A. Chan (2003), Resonant acceleration and diffusion of outer zone electrons in an asymmetric geomagnetic field, *J. Geophys. Res.*, *108*(A3), 1116, doi:10.1029/2001JA009202.

Fälthammar, C.-G. (1965), Effects of time-dependent electric fields on geomagnetically trapped radiation, *J. Geophys. Res.*, *70*(11), 2503–2516, doi:10.1029/JZ070i011p02503.

Fälthammar, C.-G. (1966a), On the transport of trapped particles in the outer magnetosphere, *J. Geophys. Res.*, *71*(5), 1487–1491, doi:10.1029/JZ071i005p01487.

Fälthammar, C.-G. (1966b), Coefficients of diffusion in the outer radiation belts, in *Radiation Trapped in the Earth's Magnetic Field*, edited by B. M. McCormac, pp. 398–402, NATO Advanced Study Institute, Netherlands.

Fälthammar, C.-G. (1968), Radial diffusion by violation of the third adiabatic invariant, in *Earth's Particles and Fields*, edited by B. M. McCormac, p. 157, NATO Advanced Study Institute, Van Nostrand Reinhold Publ. Co., New York.

Fei, Y., A. A. Chan, S. R. Elkington, and M. J. Wiltberger (2006), Radial diffusion and MHD particle simulations of relativistic electron transport by ULF waves in the September 1998 storm, *J. Geophys. Res.*, *111*, A12209, doi:10.1029/2005JA011211.

Frank, L. A. (1965), Inward radial diffusion of electrons of greater than 1.6 million electron volts in the outer radiation zone, *J. Geophys. Res.*, *70*, 3533–3539, doi:10.1029/JZ070i015p03533.

Friedel, R. H. W., G. D. Reeves, and T. Obara (2002), Relativistic electron dynamics in the inner magnetosphere—A review, *J. Atmos. Sol. Terr. Phys.*, *64*, 265–282, doi:10.1016/S1364-6826(01)00088-8.

Hartinger, M. D., D. L. Turner, F. Plaschke, V. Angelopoulos, and H. Singer (2013), The role of transient ion foreshock phenomena in driving Pc5 ULF wave activity, *J. Geophys. Res. Space Physics*, *118*, 299–312, doi:10.1029/2012JA018349.

Hasegawa, A. (1969), Drift mirror instability in the magnetosphere, *Phys. Fluids*, *12*, 2642.

Holzworth, R. H., and F. S. Mozer (1979), Direct evaluation of the radial diffusion coefficient near $L = 6$ due to electric field fluctuations, *J. Geophys. Res.*, *84*(A6), 2559–2566, doi:10.1029/JA084iA06p02559.

Huang, C.-L., H. E. Spence, H. J. Singer, and W. J. Hughes (2010a), Modeling radiation belt radial diffusion in ULF wave fields: 1. Quantifying ULF wave power at geosynchronous orbit in observations and in global MHD model, *J. Geophys. Res.*, *115*, A06215, doi:10.1029/2009JA014917.

Huang, C.-L., H. E. Spence, M. K. Hudson, and S. R. Elkington (2010b), Modeling radiation belt radial diffusion in ULF wave fields: 2. Estimating rates of radial diffusion using combined MHD and particle codes, *J. Geophys. Res.*, *115*, A06216, doi:10.1029/2009JA014918.

Jacobs, J. A., Y. Kato, S. Matsushita, and V. A. Troitskaya (1964), Classification of geomagnetic micropulsations, *J. Geophys. Res.*, *69*, 180–181, doi:10.1029/JZ069i001p00180.

Kim, K., Y. Shprits, D. Subbotin, and B. Yi (2012), Relativistic radiation belt electron responses to GEM magnetic storms: Comparison of CRRES observations with 3-D VERB simulations, *J. Geophys. Res.*, *117*, A08221, doi:10.1029/2011JA017460.

Kivelson, M. G., and C. T. Russell (Eds.) (1995), *Introduction to Space Physics*, Cambridge Univ. Press, Cambridge, U. K.
Kivelson, M. G., and D. J. Southwood (1988), Hydromagnetic waves in the ionosphere, *Geophys. Res. Lett.*, *15*, 1271–1274, doi:10.1029/GL015i011p01271.
Kletzing, C., et al. (2013), The Electric and Magnetic Field Instrument Suite and Integrated Science (EMFISIS) on RBSP, *Space Sci. Rev.*, *179*(1-4), 127–181, doi:10.1007/s11214-013-9993-6.
Lanzerotti, I. J., and C. G. Morgan (1973), ULF geomagnetic power near $L = 4$: 2. Temporal variations of the radial diffusion coefficients for relativistic electrons, *J. Geophys. Res.*, *78*, 4600–4610, doi:10.1029/JA078i022p04600.
Lanzerotti, I. J., D. C. Webb, and C. W. Arthur (1978), Geomagnetic field fluctuations at synchronous orbit: 2. Radial diffusion, *J. Geophys. Res.*, *83*, 3866–3870, doi:10.1029/JA083iA08p03866.
Lanzerotti, L. J., and M. F. Robbins (1973), ULF geomagnetic power near $L = 4$: 1. Quiet-day power spectra at conjugate points during December solstice, *J. Geophys. Res.*, *78*, 3816–3827, doi:10.1029/JA078i019p03816.
Lanzerotti, L. J., C. G. Maclennan, and M. Schulz (1970), Radial diffusion of outer-zone electrons: An empirical approach to third-invariant violation, *J. Geophys. Res.*, *75*, 5351–5371, doi:10.1029/JA075i028p05351.
Li, Z., M. Hudson, and Y. Chen (2014), Radial diffusion comparing a THEMIS statistical model with geosynchronous measurements as input, *J. Geophys. Res. Space Physics*, *119*, 1863–1873, doi:10.1002/2013JA019320.
Liu, W., W. Tu, X. Li, T. Sarris, Y. Khotyaintsev, H. Fu, H. Zhang, and Q. Shi (2016), On the calculation of electric diffusion coefficient of radiation belt electrons with in situ electric field measurements by THEMIS, *Geophys. Res. Lett.*, *43*, 1023–1030, doi:10.1002/2015GL067398.
Lyons, L. R., and D. J. Williams (1975), The quiet time structure of energetic (35–560 keV) radiation belt electrons, *J. Geophys. Res.*, *80*(7), 943–950, doi:10.1029/JA080i007p00943.
Mann, I. R., A. N. Wright, K. J. Mills, and V. M. Nakariakov (1999), Excitation of magnetospheric waveguide modes by magnetosheath flows, *J. Geophys. Res.*, *104*(A1), 333–353, doi:10.1029/1998JA900026.
Mozer, F. S. (1971), Power spectra of the magnetospheric electric field, *J. Geophys. Res.*, *76*, 3651–3667, doi:10.1029/JA076i016p03651.
Newkirk, L. L., and M. Walt (1968), Radial diffusion coefficient for electrons at $1.76 < L < 5$, *J. Geophys. Res.*, *73*, 7231–7236, doi:10.1029/JA073i023p07231.
Ozeke, L. G., I. R. Mann, K. R. Murphy, I. J. Rae, D. K. Milling, S. R. Elkington, A. A. Chan, and H. J. Singer (2012), ULF wave derived radiation belt radial diffusion coefficients, *J. Geophys. Res.*, *117*, A04222, doi:10.1029/2011JA017463.
Ozeke, L. G., I. R. Mann, K. R. Murphy, I. J. Rae, and D. K. Milling (2014), Analytic expressions for ULF wave radiation belt radial diffusion coefficients, *J. Geophys. Res. Space Physics*, *119*, 1587–1605, doi:10.1002/2013JA019204.
Perry, K. L., M. K. Hudson, and S. R. Elkington (2005), Incorporating spectral characteristics of Pc5 waves into three-dimensional radiation belt modeling and the diffusion of relativistic electrons, *J. Geophys. Res.*, *110*, A03215, doi:10.1029/2004JA010760.
Press, W. H., S. A. Teukolsky, W. T. Vetterling, and B. P. Flannery (2007), *Numerical Recipes: The Art of Scientific Computing*, 3rd ed., Cambridge Univ. Press, New York.
Roederer, J. G., and H. Zhang (2014), *Dynamics of Magnetically Trapped Particles*, Foundations of the Physics of Radiation Belts and Space Plasmas, 2nd ed., Springer-Verlag, Berlin, doi:10.1007/978-3-642-41530-2.
Schulz, M., and L. Lanzerotti (1974), *Particle Diffusion in the Radiation Belts*, Springer, New York, doi:10.1007/978-3-642-65675-0.
Selesnick, R. S., J. B. Blake, W. A. Kolasinski, and T. A. Fritz (1997), A quiescent state of 3 to 8 MeV radiation belt electrons, *Geophys. Res. Lett.*, *24*, 1343–1346, doi:10.1029/97GL51407.
Shprits, Y. Y., R. M. Thorne, G. D. Reeves, and R. Friedel (2005), Radial diffusion modeling with empirical lifetimes: Comparison with CRRES observations, *Ann. Geophys.*, *23*(4), 1467–1471, doi:10.5194/angeo-23-1467-2005.
Shprits, Y. Y., S. R. Elkington, N. P. Meredith, and D. A. Subbotin (2008a), Review of modeling of losses and sources of relativistic electrons in the outer radiation belt I: Radial transport, *J. Atmos. Sol. Terr. Phys.*, *70*, 1679–1693, doi:10.1016/j.jastp.2008.06.008.
Shprits, Y. Y., D. A. Subbotin, N. P. Meredith, and S. R. Elkington (2008b), Review of modeling of losses and sources of relativistic electrons in the outer radiation belt II: Local acceleration and loss, *J. Atmos. Sol. Terr. Phys.*, *70*, 1694–1713, doi:10.1016/j.jastp.2008.06.014.
Slepian, D. (1978), Prolate spheroidal wave functions, Fourier analysis, and uncertainty—V: The discrete case, *Bell Syst. Tech. J.*, *57*, 1371–1430, doi:10.1002/j.1538-7305.1978.tb02104.x.
Southwood, D. J., J. W. Dungey, and R. J. Etherington (1969), Bounce resonant interaction between pulsations and trapped particles, *Planet. Space Sci.*, *17*, 349–361, doi:10.1016/0032-0633(69)90068-3.
Squires, G. L. (2001), *Practical Physics*, 4th ed., Cambridge Univ. Press, Cambridge, U. K.
Su, Z., F. Xiao, H. Zheng, and S. Wang (2010), STEERB: A three-dimensional code for storm-time evolution of electron radiation belt, *J. Geophys. Res.*, *115*, A09208, doi:10.1029/2009JA015210.
Su, Z., F. Xiao, H. Zheng, and S. Wang (2011a), CRRES observation and STEERB simulation of the 9 October 1990 electron radiation belt dropout event, *Geophys. Res. Lett.*, *38*, L06106, doi:10.1029/2011GL046873.
Su, Z., F. Xiao, H. Zheng, and S. Wang (2011b), Radiation belt electron dynamics driven by adiabatic transport, radial diffusion, and wave-particle interactions, *J. Geophys. Res.*, *116*, A04205, doi:10.1029/2010JA016228.
Subbotin, D. A., Y. Y. Shprits, M. Gkioulidou, L. R. Lyons, B. Ni, V. G. Merkin, F. R. Tofoletto, R. M. Thorne, R. B. Horne, and M. K. Hudson (2011a), Simulation of the acceleration of relativistic electrons in the inner magnetosphere using RCM-VERB coupled codes, *J. Geophys. Res.*, *116*, A08211, doi:10.1029/2010JA016350.
Subbotin, D. A., Y. Y. Shprits, and B. Ni (2011b), Long-term radiation belt simulation with the VERB 3-D code: Comparison with CRRES observations, *J. Geophys. Res.*, *116*, A12210, doi:10.1029/2011JA017019.
Tascione, T. F. (1988), *Introduction to the Space Environment*, Orbit Book Company Inc., Malabar, Fla.
Thomson, D. J. (1982), Spectrum estimation and harmonic analysis, *Proc. IEEE*, *70*, 1055–1096, doi:10.1109/PROC.1982.12433.
Treumann, R. A., and W. Baumjohann (1997), *Advanced Space Plasma Physics*, Imperial College Press, London.
Tsyganenko, N. A., and M. I. Sitnov (2005), Modeling the dynamics of the inner magnetosphere during strong geomagnetic storms, *J. Geophys. Res.*, *110*, A03208, doi:10.1029/2004JA010798.
Tu, W., X. Li, Y. Chen, G. D. Reeves, and M. Temerin (2009), Storm-dependent radiation belt electron dynamics, *J. Geophys. Res.*, *114*, A02217, doi:10.1029/2008JA013480.
Tu, W., S. R. Elkington, X. Li, W. Liu, and J. Bonnell (2012), Quantifying radial diffusion coefficients of radiation belt electrons based on global MHD simulation and spacecraft measurements, *J. Geophys. Res.*, *117*, A10210, doi:10.1029/2012JA017901.
Tu, W., G. S. Cunningham, Y. Chen, M. G. Henderson, E. Camporeale, and G. D. Reeves (2013), Modeling radiation belt electron dynamics during GEM challenge intervals with the DREAM3D diffusion model, *J. Geophys. Res. Space Physics*, *118*, 6197–6211, doi:10.1002/jgra.50560.
Ukhorskiy, A. Y., B. J. Anderson, K. Takahashi, and N. A. Tsyganenko (2006), Impact of ULF oscillations in solar wind dynamic pressure on the outer radiation belt electrons, *Geophys. Res. Lett.*, *33*, L06111, doi:10.1029/2005GL024380.

Varotsou, A., D. Boscher, S. Bourdarie, R. Horne, N. P. Meredith, S. A. Glauert, and R. H. Friedel (2008), Three-dimensional test simulations of the outer radiation belt electron dynamics including electron-chorus resonant interactions, *J. Geophys. Res.*, *113*, A12212, doi:10.1029/2007JA012862.

West, I. H., R. M. Buck, and G. T. Davidson (1981), The dynamics of energetic electrons in the Earth's outer radiation belt during 1968 as observed by Lawrence Livermore National Laboratory's spectrometer on Ogo 5, *J. Geophys. Res.*, *86*, 2111–2142, doi:10.1029/JA086iA04p02111.

Wygant, J., et al. (2013), The electric field and waves instruments on the Radiation Belt Storm Probes Mission, *Space Sci. Rev.*, *179*(1–4), 183–220, doi:10.1007/s11214-013-0013-7.

Zheng, L., A. A. Chan, J. M. Albert, S. R. Elkington, J. Koller, R. B. Horne, S. A. Glauert, and N. P. Meredith (2014), Three-dimensional stochastic modeling of radiation belts in adiabatic invariant coordinates, *J. Geophys. Res. Space Physics*, *119*, 7615–7635, doi:10.1002/2014JA020127.